Original Research Article

Numerical assessments of observed seismic performances of Lexington Dam during the 1989 Loma Prieta earthquake

Ashok K. Chugh

U.S. Bureau of Reclamation Denver, Colorado 80225,
*Corresponding author： *USA achugh@usbr.gov*

Abstract: Seismic performances of Lexington Dam during the 1989 Loma Prieta earthquake are assessed. Linear and nonlinear analyses are used to identify locations of tension zones where cracks are likely to occur. Numerical analyses are for longitudinal and transverse sections of the dam. Assessments of natural vibration characteristics of the dam are based on numerical simulation of geophysical and forced vibration testing procedures. Nonlinear analyses are based on equivalent linear and elastoplastic solution procedures. The acronyms of computer programs used are SHAKE, SHAKEM and FLAC. Analyses procedures and computer programs used are commonly used in dam engineering practice. Relative movements of observers representing onsite accelerometers are included. The information presented is expected to be of interest to engineers and seismologists in dam engineering practice.

Keywords: Earthquake awareness, Equivalent linear, Dam engineering.

1. Introduction

Study of case histories of dam incidents and failures is an important part of analysis and design. Lessons learned from case histories lead to improvements in analysis and design practices and procedures which result in construction of safe and reliable structures. Dams are considered critical structures and their integrity and safe reservoir operations are of importance to ensure public safety and wellbeing. All constructed facilities are designed to safely withstand service loads which include (a) self-weight of the structure, (b) loads from intended uses of the facility, and (c) allowance for known but unpredictable sources such as earthquakes and other natural events. Details of natural-event loads are not known as a priori. For a known site of an existing or proposed structure, seismologists develop seismic motions that are used by engineers to analyze and design the structure with certain margin of safety to allow for uncertainties in the predicted seismic motions, and other unknowns. Because earth-sciences based disciplines rely on limited knowledge of subsurface geologic and tectonic conditions, seismologists and engineers make assumptions in their work. Actual motions experienced at a project site are invariably different from the ones predicted prior to the event.

There are relatively few case studies on assessments of seismic performance of earth dams in which (i) ground motions were large such as the ones induced by a strong earthquake; (ii) the earthquake source was close to the damsite; (iii) there were appropriate onsite seismic instrumentation in terms of their locations on the dam and types of accelerometer sensors which detect and record seismic waves; (iv) seismic instruments at the dam site had functioned properly; (v) the dam had survived the strong motion event; and (vi) performances of the facility had provided useful data in terms of deformations and cracks[1-3]. The October 17, 1989 Loma Prieta earthquake was a significant seismic event in terms of its severity that had caused extensive damages to dams, buildings, roads and bridges, and other infrastructure facilities. Lexington Dam was one of the several earth dams affected by the 1989 Loma Prieta earthquake[4]. There are number of publications describing post-seismic analyses of the Lexington Dam[5-8]. In these studies, the dam was analyzed using (i) 2- or 3- dimensional models; (ii) equivalent linear or plasticity based non-linear material models of varying complexity;

(iii) estimated and measured material properties; (iv) different saturation conditions; and (v) different dynamic excitations. The computed results are explained to be reasonable.

Because of the unusually large displacements and extensive cracking of Lexington Dam during the 1989 Loma Prieta earthquake, a somewhat different approach is taken in the work included in this paper. Seismic response of a dam during an earthquake is considered to be the result of an interplay between two independent vibrating entities. Dam is one of the two entities which is vibrating all the time at its natural frequencies (free vibrations); and earthquake motion is the second independent entity which is made up of a series of waves composed of different frequencies. During a seismic event, the seismic waves exert external time varying forces on the dam and affect its prevalent vibration modes. Details of free and forced vibrations, and consequences of their interactions in terms of deformations and locations of tension zones for the Lexington Dam are of interest in this study. Specifically, the following details are included in this paper:

(1) analyses of the seismic motions recorded at the dam site in terms of their frequency content;

(2) computations of natural vibration characteristics (frequencies and mode shapes) of the dam and identification of tension zone locations;

(3) deconvolutions of the recorded motions in the upstream-downstream and the dam-axis directions using 1-D wave propagation analyses based on viscoelastic material model;

(4) computed results of permanent displacements and tension zones using motions developed in (c);

(5) comparisons of results from (1) to (4) amongst themselves and with the field data.

The results included in the paper are based on information from California Department of Water Resources data about the dam, reservoir water levels, and material properties that existed prior to the occurrence of the earthquake[9-11]. Numerical models used are one- and two- dimensional representations of the prototype dam sections in the longitudinal (dam-axis) and transverse (upstream-downstream) directions. Constitutive material models used are linear elastic, (ii) viscoelastic, and (iii) nonlinear elastoplastic with Mohr-Coulomb yield criterion. All three material models are used in two-dimensional (2-D) continuum analyses; viscoelastic material model is used in one-dimensional analyses. Equivalent-linear method is used to simulate hysteretic response of viscoelastic material under cyclic loading.

Two-dimensional models represent the prototype dam sections; 1-D models represent the dam in the longitudinal and transverse directions – height of the 1-D models equals the height of the dam at their respective locations; and width of the models equals the width of layers in the transverse section, and the width of the numerical model for the longitudinal section. The computer programs used are: SHAKEM[12], and FLAC[13]. SHAKEM is a modified version of the computer program SHAKE[14]; FLAC is an acronym for Fast Lagrangian Analysis of Continua (Itasca Consulting Group, 2011). Natural frequencies of the dam are calculated by applying a dynamic force varying in the form of a high frequency and short duration sine pulse at the dam crest – similar to the hammer-blow used in crosshole/downhole seismic surveys, see [15] for details. Natural mode shapes of the dam are calculated by applying a dynamic force varying in the form of a continuous sine wave of a resonant frequency and long duration at the dam crest – similar to the forced vibration tests using eccentric-mass vibratory shakers to determine dynamic response characteristics of structures, see [16-18] for details.

The computer program FLAC solves the equation of motion in time domain, and the output results are in time domain. The computer program SHAKE (or SHAKEM) solves the wave equation in frequency domain, and the output results are in time domain. The results in time-domain were converted to their frequency-domain equivalents via Fourier transforms. All vibration related analyses of Lexington Dam were performed in time domain and results converted to frequency domain using the Fast Fourier transform (FFT) algorithm available in FLAC software.

2. Rationale for Material Models Used

Linear elastic material model assumption used in the analyses is a sequel to [19,20] report where it is demonstrated that the tension zones identified by its use on planar longitudinal sections of four earth and rockfill dams (which had cracked or in which large tension zones had developed) were in good agreement with the observations. In the analyses, the only load considered was the weight of the dam, and it was assumed to be applied in a single lift. It was recognized that the assumption of linear elastic material, with equal properties in tension and compression, exaggerated the development of tension zones.

Equivalent linear method used for analyses is a continuation of its traditional and worldwide use in analyses of earth and rockfill dams during 1970-1990. It was used for deconvolution of recorded data in SHAKE and

SHAKEM analyses, and as an alternate to the elastoplastic material model. The nonlinearity of the shear modulus and damping is accounted for by the use of equivalent linear soil properties.

Elastoplastic material model with Mohr-Coulomb yield criterion used for permanent displacements and tension zones is a commonly used material model in dam engineering practice.

Continuum-mechanics based analyses procedures are not applicable for study of development and propagation of cracks in solids – fracture-mechanics based procedures are needed for the cracking issues; see [21] for details. However, locations of tension zones identified via a continuum- mechanics based analysis of a dam are good indicators of where cracks are likely to develop. FLAC is a continuum-mechanics based analysis program.

2.1 Lexington Dam Description

Lexington Dam (now known as James J. Lenihan Dam) is a 64 m high, 247 m long zoned earth dam located in a seismically active region of California in the Western United States. The dam crest is about 12 m wide. The u/s slope of the dam is 5.5H:1V and the d/s slope is 3H:1V. The dam is sited in a narrow valley with side slopes of about 2H:1V. Instrumentation at the dam site include: three strong motion instruments (accelerometer), nine survey monuments (MON), and three observation wells (OW) – two of the accelerometers are located on the dam crest and the third is on the left abutment; the nine MONs are located along the dam crest at about 30 m spacings; and the three OWs are located along the downstream (d/s) toe of the dam. Figure 1 shows the site-specific details of the dam. The dam was constructed in 1952 and the facility put into service in 1956. The dam is owned and operated by the Santa Clara Valley Water District. The project data are in Imperial units and all analyses were performed in these units; for this paper, the Imperial units were converted to SI units and conveniently rounded.
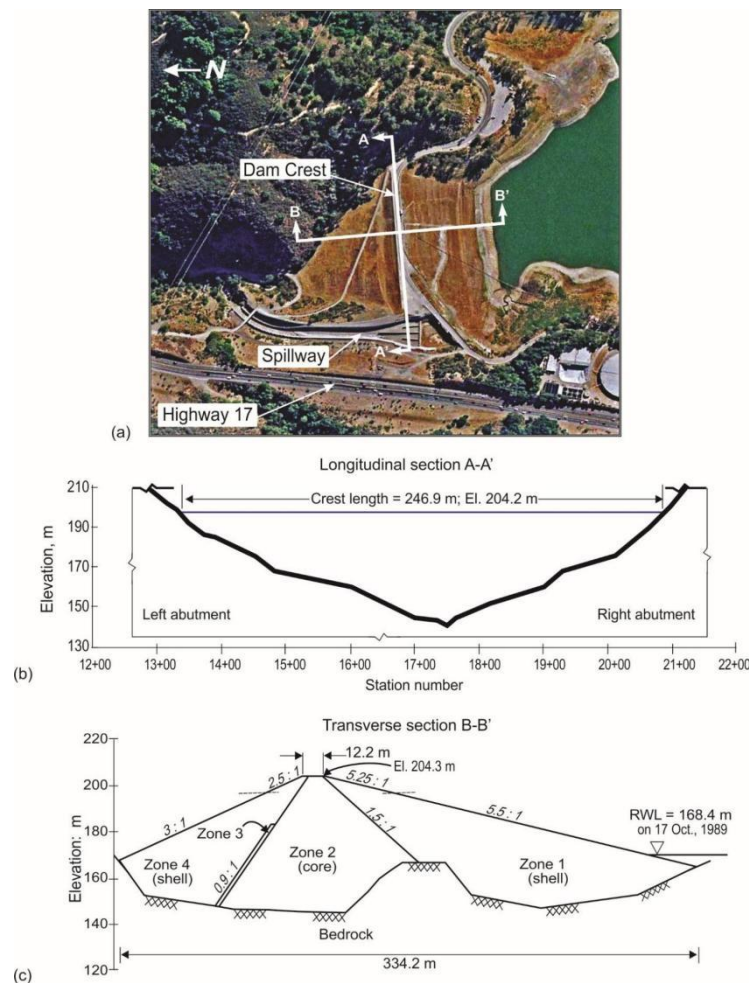
Figure 1. Site specific details of Lexington Dam, [10]: (a) aerial view; (b) profile view of the valley along the dam axis; (c) cross section view of the dam (d) instrumentation locations; (e) water level data from 1981 to 1990.
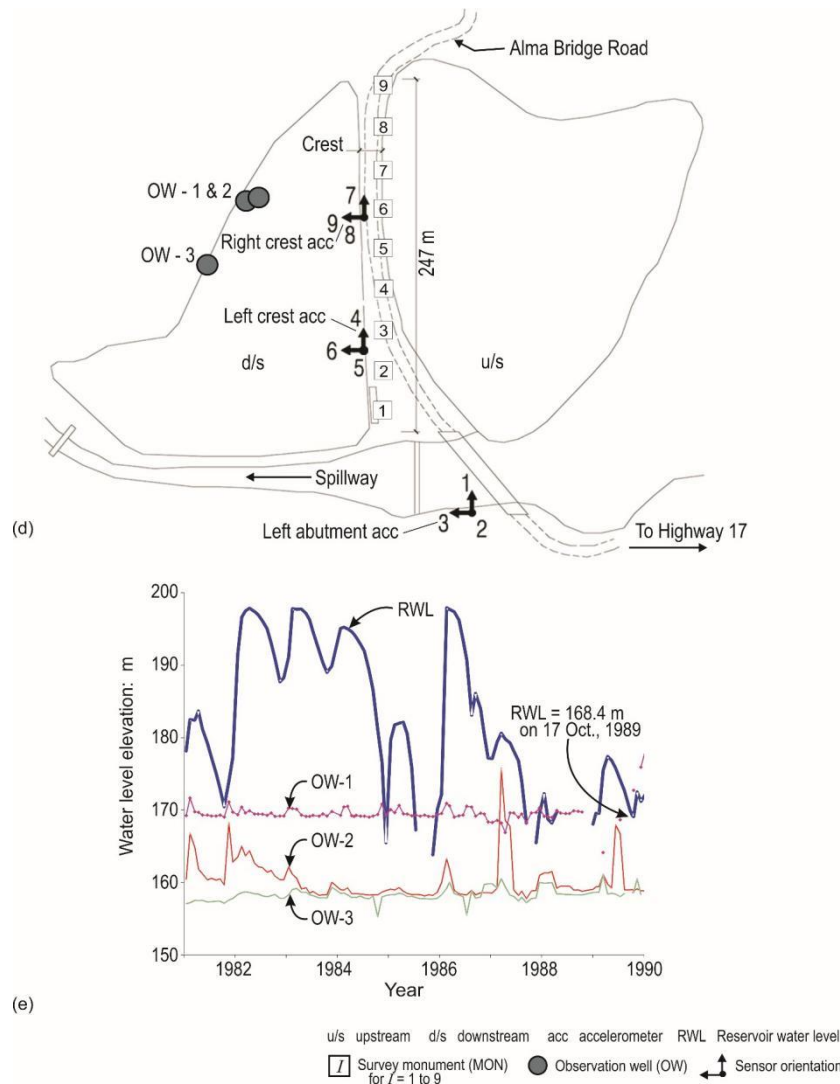
Figure 1. **(Continued)**

2.2 Seismic Event

On October 17, 1989, the dam site experienced the Loma Prieta earthquake of magnitude 6.9 (Mw 6.9) and a maximum Modified Mercalli intensity of IX (violent). The spatial coordinates of the earthquake epicenter are 37.037°N, 121.883°W. Lexington Dam is located about 21 km north-west of the earthquake epicenter; the spatial coordinates of the dam are: 37.202°N, 121.949°W. Figure 2(a) shows the relative locations of the dam and the epicenter of the earthquake. All three strong motion instruments at the dam site recorded time-acceleration histories during the seismic event – CSMIP[22]; COSMOS[23]. Figures 2(b-d) show plots of the recorded motions in three orthogonal directions at each of the seismic instrument location; see Fig. 1(d) for the accelerometer sensor identifications number (ID #) and its orientation with respect to the dam reference terminology (longitudinal, transverse, and vertical) – for example sensors 1, 2 and 3 are for the accelerometer located on the left abutment, and the time-acceleration data recorded by sensor 1 are in the dam-axis (longitudinal) direction. Accelerometer locations are identified as left abutment, left crest, and right crest. Peak accelerations from the dam crest instrument recordings were up to about: 0.39g longitudinal (dam-axis direction), 0.21g vertical (up-down direction), and 0.45g transverse (u/s-d/s direction). The corresponding peak accelerations at the left abutment instrument were: 0.41g, 0.13g, and 0.44g, respectively. A summary of peak accelerations at the three seismic stations is shown in Table 1. The peak velocity and displacement values are shown in Tables 2 and 3, respectively. COSMOS[23] shows plots of data. and CSMIP[22] includes digital data.
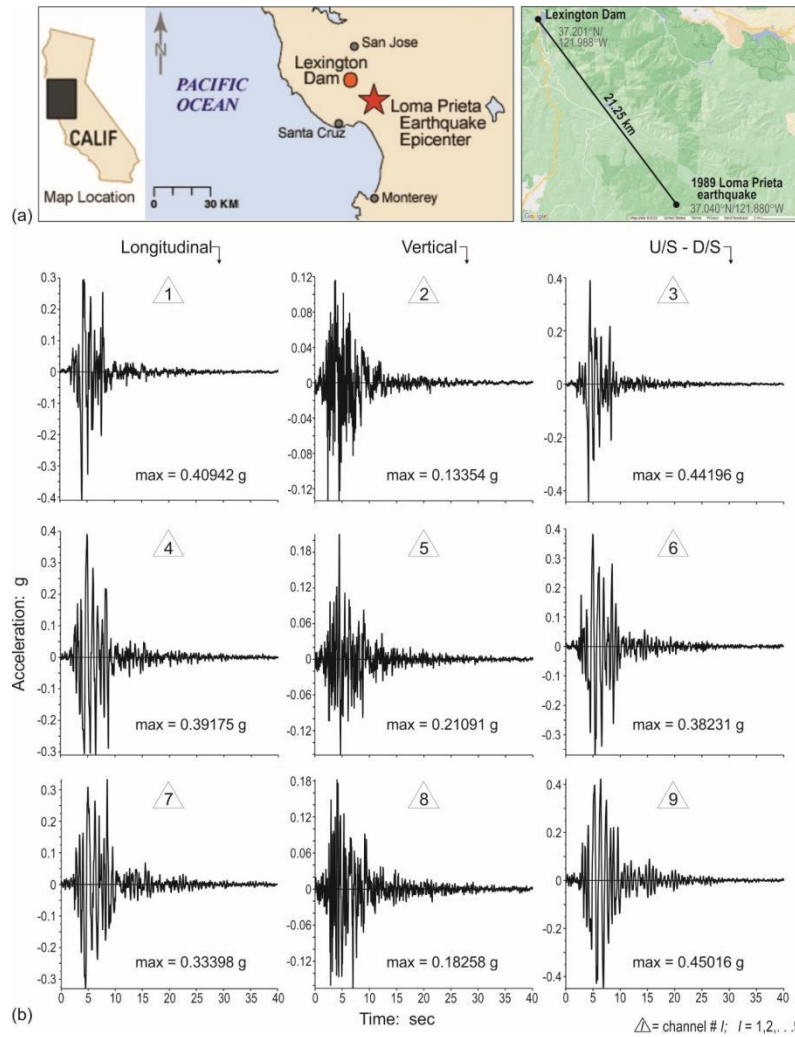
Figure 2. Details for the October 17, 1987 Loma Prieta earthquake: (a) Relative locations of the Lexington Dam and earthquake epicenter; (b) time-acceleration data recorded by accelerometers at left abutment, left crest, and right crest locations; (c) time-velocity data corresponding to (b); (d) time-displacement data corresponding to (c); (e) measured displacements of survey monuments in vertical and transverse directions; and (f) aerial view of the surface crack locations and extent, [10].

The sensor orientations shown in Fig. 1(d) imply: the longitudinal direction is positive towards the right abutment; transverse direction is positive towards the d/s; and vertical direction is positive towards the up. Terms left and right are with respect to an observer looking downstream.

Table 1   Recorded peak accelerations at Lexington Dam during the 1989 Loma Prieta earthquake

Instrument location	Peak recorded acceleration: g		
	Station Channel ID # / dam reference direction		
	1, 4, 7dam-axis	2, 5, 8vertical	3, 6, 9u/s – d/s
Left abutment	-0.4094	-0.1335	-0.4420
Crest (left)	0.3917	0.2109	0.3823
Crest (right)	0.3340	0.1826	-0.4502

Table 2   Peak velocities of the recorded accelerations data

Instrument location ID	Peak velocity: cm/s		
	1, 4, 7dam-axis	2, 5, 8vertical	3, 6, 9u/s-d/s
Left abutment	-94.982	25.526	-84.434
Crest (left)	-102.971	31.328	-76.683
Crest (right)	-104.406	26.337	-86.611
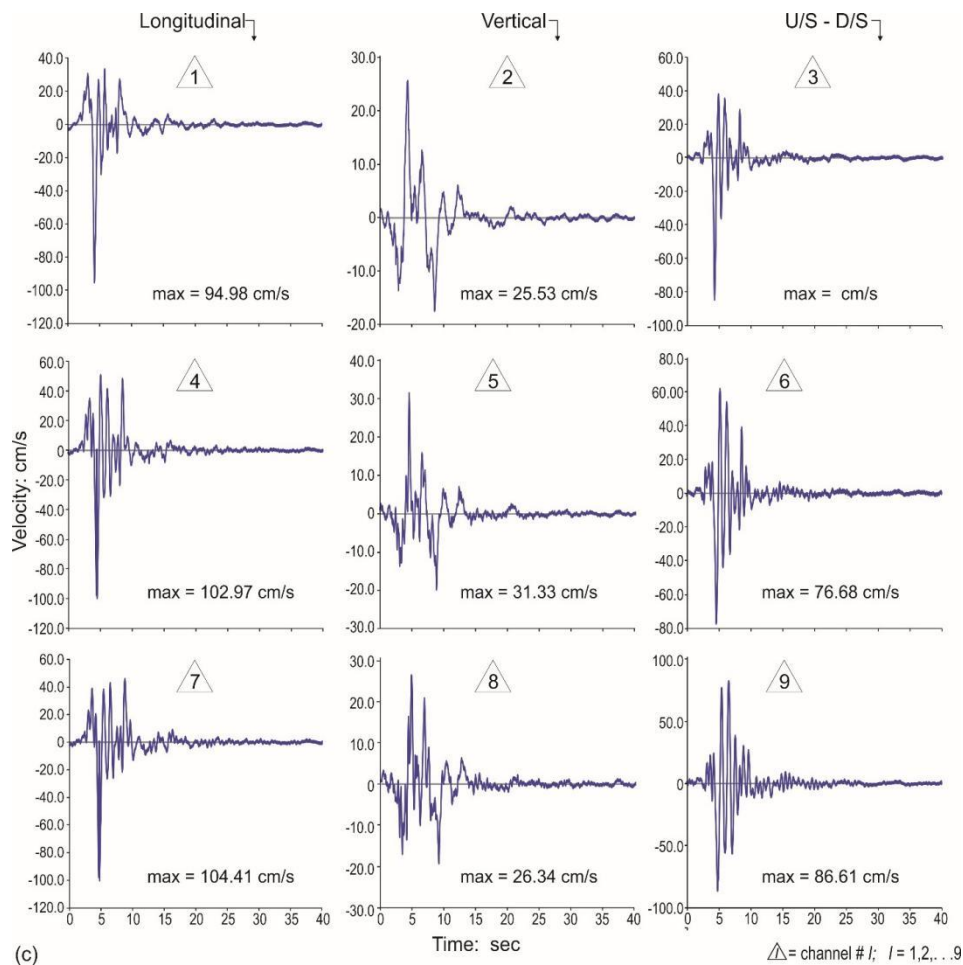
Figure 2.   (Continued)

Table 3   Peak displacements of the recorded accelerations data

Instrument location ID	Peak displacement: cm		
	1, 4, 7dam-axis	2, 5, 8vertical	3, 6, 9u/s-d/s
Left abutment	25.814	13.080	14.673
Crest (left)	26.422	9.516	19.141
Crest (right)	27.540	10.819	24.145

Peak values of acceleration, velocity, and displacement occur at different times in the recorded data.

It is significant to note that each of the three accelerometers data have high amplitude (acceleration) and relatively larger duration (time) pulses in the u/s-d/s and dam-axis directions as compared to the time-acceleration data in the vertical direction; the sustained durations are from about time 4 to 10 s in the crest instruments data and from about 3 to 7 s in the left abutment data.

2.3 Observed Performance After The Seismic Event

Permanent displacements: The dam crest had experienced large permanent settlements (vertical displacements) as compared to the transverse displacements along the length of the dam – maximum settlement was about 26 cm near station 17+00, and the maximum transverse displacement was about 8 cm d/s near station 16+00. The transverse displacements are towards the d/s between dam stations 13+00 and 19+00, and towards the u/s between dam stations 19+00 and 21+10. It is not known if permanent deformations in the dam-axis direction had occurred or not occurred. Figure 2I shows the results from the post-seismic surveys of the dam site; numerical values of the plotted displacements are listed in Table 4.
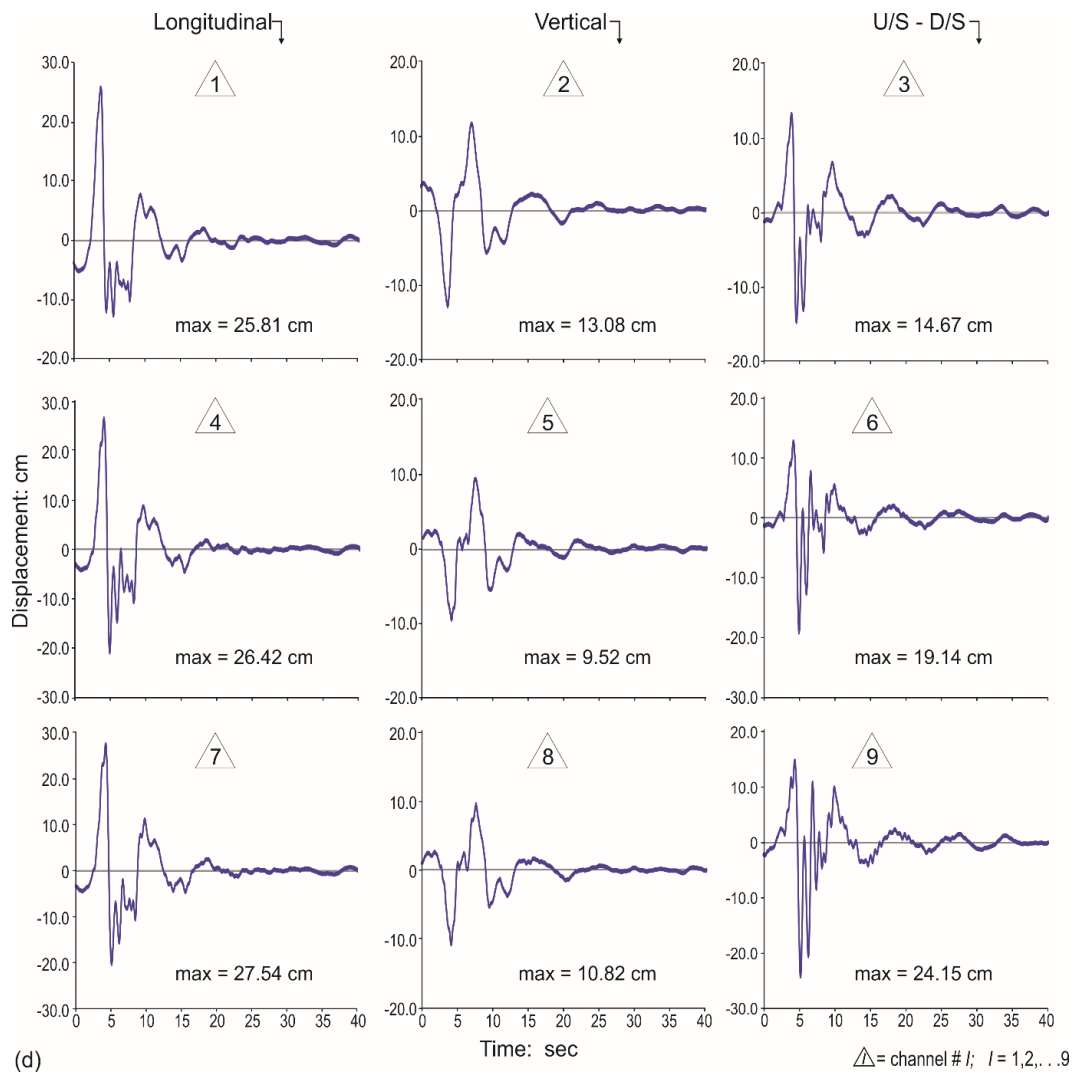
Figure 2. **(Continued)**
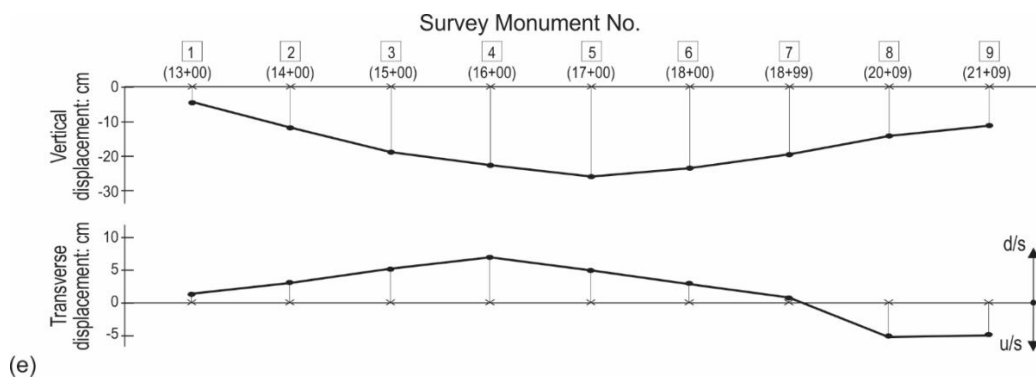
Figure 2. **(Continued)**

Table 4. Summary of permanent displacements along the dam axis; [7]

Permanent displacements	Survey monument number (closest dam station number)							
	1(13+00)	3(15+00)	4(16+00)	5(17+00)	6(18+00)	7(19+00)	8(20+00)	9(21+10)
Settlement: cm	-4.57	-18.59	-22.55	-25.91	-23.77	-19.20	-14.02	-10.67
u/s – d/s: cm	0.91	6.40	7.62	5.49	3.05	-0.30	-3.66	-3.66

Settlements are downwards; positive transverse displacements are towards the d/s, and the negative transverse displacements are towards the u/s.

Dam Cracks: The overall response of the dam had resulted in extensive transverse cracks near both abutments, and localized longitudinal cracks on the u/s and d/s slopes of the dam. Field investigations had revealed the cracks to be up to about 2 cm wide×215 cm deep. Figure 2(f) shows the aerial view of the locations, and traces of surface cracks[7, 8, 10].

The observed cracks are considered tension cracks because the crack surface moved directly apart without a vertical offset; the movement is caused by tensile forces normal to the faces of the crack[19].

Crack types: The observed cracks are extensional type which are caused by tensile forces normal to the faces of the crack and can occur under plane stress or plane strain conditions. These are termed tension cracks in this writeup.

Another type of crack in earth dams is a shear crack in which the crack surfaces slide over each other in the direction perpendicular to the leading edge of the crack. Shear cracks are caused by shear stresses in the direction of movement and can occur under plane stress or plane strain conditions. Since there was no slip failures in the Lexington Dam, no slope stability analyses were performed for this case study. The tension cracks are classed as Mode I cracks; the shear cracks are classed as Mode II cracks in [19].

2.4 Visualization of the Relative Movements

The displacement data of the recorded motions at the three seismic instrument locations are used to visualize the vibratory interactions between the abutment and the dam. Three observers, one at each of the three accelerometer locations, are located along the dam axis at the dam crest. For ease of display, the three observers are assigned the following initial coordinates: (0,0,0) to the observer at the left abutment instrument location; (100,0,0) to the observer at the left crest instrument location; and (200,0,0) to the observer at the right crest instrument location; the coordinate directions correspond to the three orthogonal directions of the accelerometer channel directions (1,2,3), (4,5,6), and (7,8,9), respectively. The recorded displacement in the respective coordinate directions were added to the assigned initial coordinates to locate the observers' positions in space in increments of 0.02 s (same as the data acquisition rate). For each time t_i (for i = 1,2000), a graph was created to see the relative positions of the three observers (identified using colored dots) in (a) a vertical plane (showing positions in the dam-axis and vertical directions), and (b) a horizontal plane (showing positions in dam-axis and u/s-d/s directions). The individual graphs were used to create real time animations of the relative positions of the observers in the horizontal and vertical planes. A copy of the animations is included in the supplemental material. The animation shows (i) the dam-abutment system experienced several excursions into higher modes of deformation in the up-down direction and in the stream direction; and (ii) the dam and abutments affected each other's response during the seismic event.

2.5 Terminology and Sign Conventions Used

Terms sensor #, station channel #, channel # are used interchangeably – they all refer to the sensor numbers shown in Fig. 1(d); for example: CH 5 refers to the sensor 5 in the accelerometer located on the left crest and is oriented in the up (vertical) direction. Similarly, terms (a) dam-axis and longitudinal; (b) upstream (u/s)-downstream (d/s) and transverse; and (c) vertical, up-down, and up are used interchangeably.

FLAC is a continuum-mechanics based computer program and uses the convention of tension positive and compression negative. SHAKE is a geomechanics based computer program and uses the convention of tension negative, and compression positive. SHAKEM is a modified version of SHAKE and follows the sign conventions used in SHAKE.

The dam stationing begins with 13+00 at the spillway structure right wall and ends with 21+10 at the right abutment; the dam stationing is in imperial units (100 ft or 30.48 m apart), thus dam length is approximately 247 m (8.10×30.48 m). Left abutment instrument is located about 85 m left of dam station 13+00; the left crest instrument is located near dam station 15+00; and the right crest instrument is located near dam station 17+75; see Fig. 1(d).

(f)
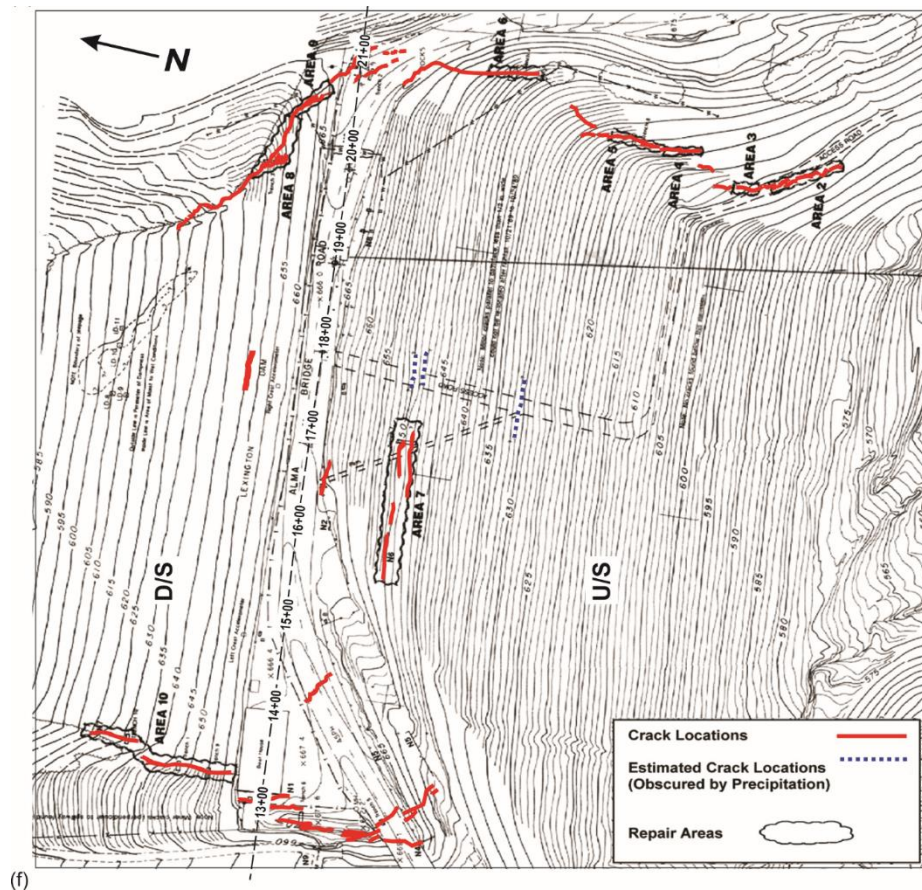
Figure 2.   (Continued)

2.6 Seismic Data Used

The basic measurements of ground motions for dynamic analyses are horizontal accelerations; velocity and displacements are derived by successive integration of acceleration data. Vertical motions are seldom used in dynamic analyses. Horizontal accelerations data in the dam-axis and u/s-d/s directions were used in the analyses included herein.

It should be mentioned that ground velocity is often more useful in correlation with structural damage, and ground displacements have a direct relationship with the strains to which large structures such as dams might be subjected, (Hudson, 1970). In addition, the frequency content, and duration of strong motion may be more pertinent than acceleration as qualifiers of damage potential during earthquakes. Assessments of frequency content of the seismic data and natural frequencies of the dam are included herein.

2.7 Analyses of the Recorded Motions Data

Fourier transforms of acceleration data: The recorded motions are for 40 seconds and contain 2000 points – this gives a sampling rate of 50 readings/sec. The highest useful frequency in the recorded data is 25 Hz (one-half of the sampling rate, known as Nyquist frequency).

Frequencies of different wave forms in the recorded motions are calculated using the Fast Fourier transforms (FFTs) of the time-series data shown in Fig. 2(b). The results are shown in Figs. 3(a-c). The spikes in the FFT spectrum plots correspond to the frequencies in the time-acceleration data recorded by the accelerometers at the dam crest and left abutment; the Fourier amplitude scale represents the amplitudes of the waves associated with the frequencies. For illustration, frequency corresponding to the tallest spike in each of the nine FFTs is listed in Table 5.

For an undamped, elastic model, a resonant frequency wave shall produce increasing displacements during the duration of the wave, and the deformed shape shall have nodes of zero displacement.
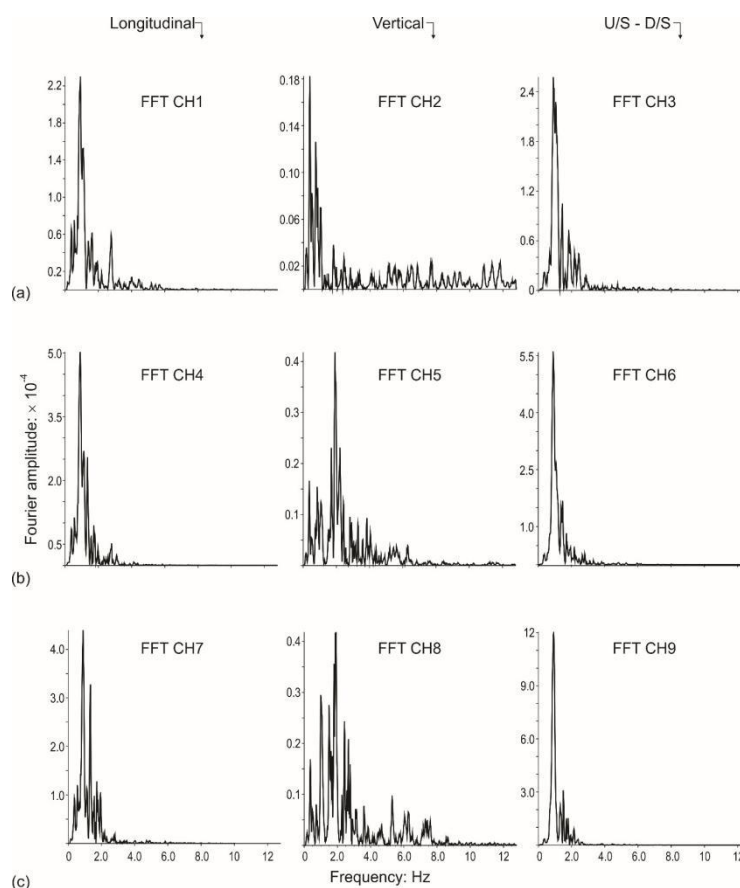
Figure 3. Fourier transform of the recorded time-acceleration data, Fig. 2(b), using Fast Fourier Transform (FFT): (a) left abutment, (b) left crest, and (c) right crest.

Table 5. Frequencies corresponding to the tallest spikes in FFT: Hz; (Fig. 3)

Instrument location ID	Frequency corresponding to the tallest spike in FFT: Hz		
	1, 4, 7 dam-axis	2, 5, 8 vertical	3, 6, 9 u/s-d/s
Left abutment	0.900	0.375	1.0
Crest (left)	0.925	1.920	0.900
Crest (right)	0.900	1.920	0.900

Fourier amplification spectrum: Amplifications of motions between the left abutment instrument data and the two crest instruments data are shown in Figs. 4(a, b). These results are obtained by dividing the FFT of crest instrument data with the FFT of corresponding data for the left abutment. Specifically, graphs in Fig. 4(a) are plots of FFT CH4/FFT CH1; FFT CH5/FFT CH2; and FFT CH6/FFT CH3. Similarly, graphs in Fig. 4(b) are plots of FFT CH7/FFT CH1; FFT CH8/FFT CH2; and FFT CH9/FFT CH3. For brevity, FFT of a recording channel is referred to as FFT followed by the channel number. For example: FFT CH1 refers to FFT of CH1.

Figure 4(c) is an overlay of graphs in Fig. 4(a) and Fig. 4(b). Based on the results shown in Fig. 4(c), if the left abutment accelerometer data were for an instrument located at the base of the dam or used as a seismic excitation (dynamic load) , the 1st resonant frequency of the dam would be about 1.3 Hz in the dam-axis direction; about 1.1/1.2 Hz in the vertical direction; and about 1.3 Hz in the u/s-d/s direction; higher resonant frequencies correspond to the frequencies associated with subsequent spikes – for example: the 2nd resonant frequencies in the respective directions would be 1.7, 1.6, and 1.5 Hz.

It should be mentioned that (i) frequencies associated with each spike, regardless of its amplitude, is a potential resonant frequency unless proven otherwise by the mode shape analysis included in the Natural vibration characteristics; and (ii) a sine wave of a non-resonant frequency shall not produce a valid displacement

and mode shape pattern.
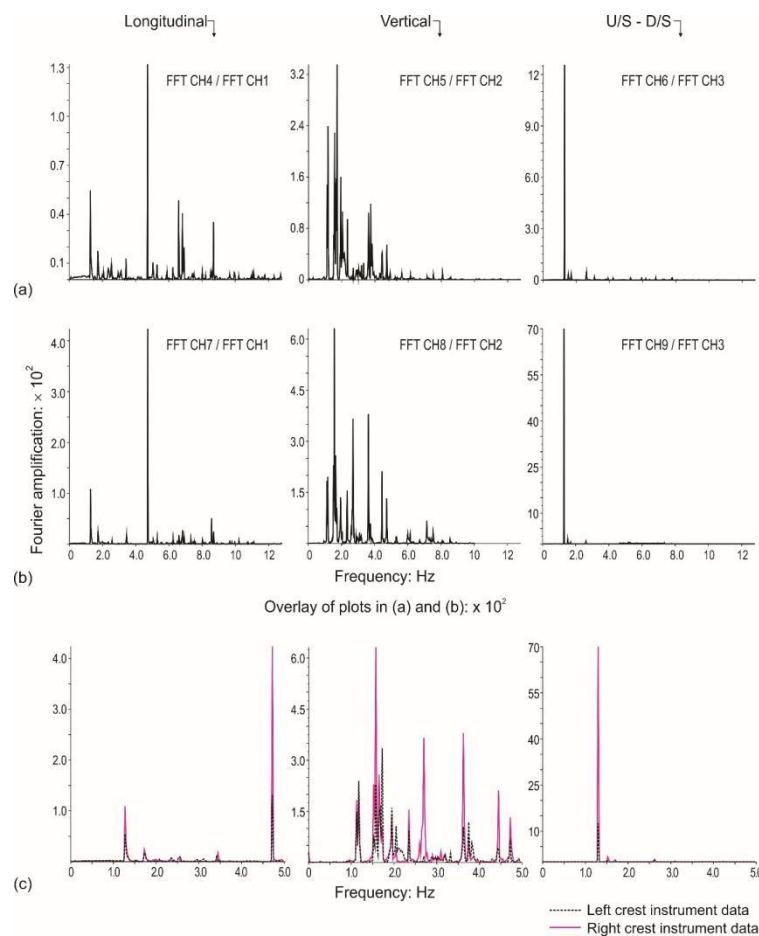
Figure 4. Fourier amplifications spectrum of crest acceleration data with-respect-to the left abutment acceleration data and their overlays: (a) left crest; (b) right crest; (c) overlays of Fourier amplification spectrum in (a) and (b).

2.8 History of Seismic Events Affecting The Dam Site

Since the construction of dam in 1954, there have been twelve earthquakes of magnitude greater than 5 within 50 km of the Lexington Dam site – the October 17, 1989 Loma Prieta earthquake was the 13th. A summary listing of these events is shown in Table 6 (USGS earthquake database: https://earthquake.usgs.gov/earthquakes/search/).

Table 6   Earlier earthquakes

Date	Magnitude	Distance (km)
April 25, 1954	5.3	40
September 5, 1955	5.5	26
March 2, 1959	5.3	42
September 14, 1963	5.4	48
November 16, 1964	5.0	30
December 18, 1967	5.3	29
August 6, 1979	5.9	44
April 24, 1984 (Morgan Hill)	6.2	28
March 31, 1986	5.7	40
June 13, 1988	5.4	27
June 27, 1988	5.7	12
August 8, 1989	5.4	8
October 17, 1989 (Loma Prieta)	7.1	20

There were no reported damages to the Lexington Dam or its appurtenant structures for these events. The October 17, 1989 Loma Prieta earthquake was the most severe seismic event affecting the Lexington Dam site.

3. Site geology and Material Properties

Site geology: There is limited documentation of foundation conditions after the completion of foundation excavations (prior to placement of the dam materials). The dam is located in the upper reaches of Los Gatos Creek. The valley walls on the right side of the dam are relatively smooth; the valley walls on the left side of the dam are irregular due to the presence of massive rock knobs; and the valley floor has bedrock knobs. The dam is founded on Franciscan sandstone and shale with minor amounts of greenstone, chert, and schist – the surface deposits were removed prior to placement of the dam materials. Thus, the observed performances of the dam are not due to loss of strength in the dam foundation materials [6]. The dam site is in an active tectonic region with major faults in proximity to the dam. See [25] for details.

Geophysical data: Figure 5(a) shows the shear wave velocity data based on downhole and crosshole seismic wave velocity measurements in the central core zone 2, and u/s and d/s shell zones[11]. These data were used to calculate initial shear modulus, G_{max}, of different zone materials in the dam.

(a)

(b)

(c)
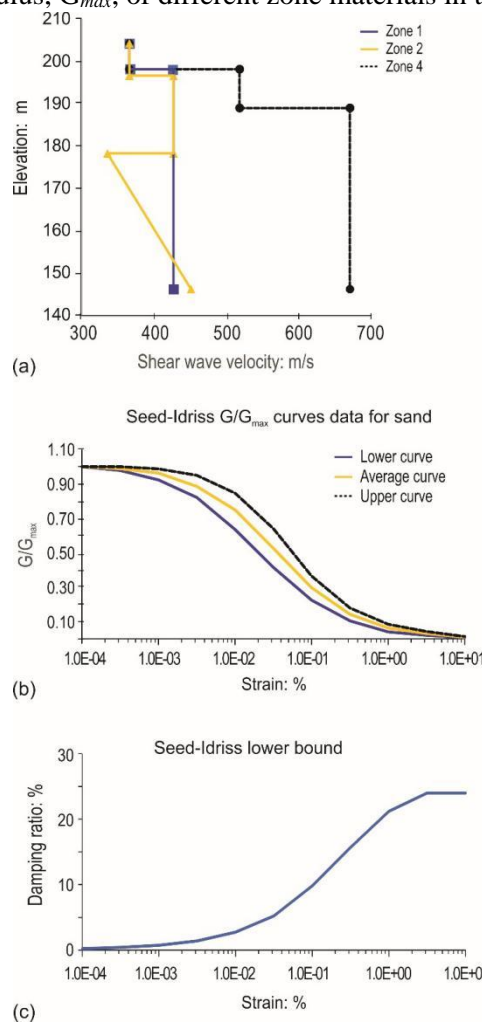
Figure 5. Geophysical test results and cyclic stress-strain parameters used for dynamic analyses: (a) shear wave velocity data, [11]; (b) shear modulus vs cyclic shear strain data, and (c) damping ratio vs cyclic shear strain data, [26].

Material properties: Lexington Dam is a well compacted zoned earthfill structure, Fig. 1(c). Excavated materials from dam foundation, outlet works, spillway, and a nearby borrow site were used in u/s zone 1; clay loams with varying amounts of gravels were used in impervious zone 2 core; large free draining gravely material were used for the zone 3 drain; and semi-impervious materials were used in d/s zone 4. Based on boring logs,

laboratory and field tests, the impervious zone 2 material is assigned different properties above and below El. 180 m. Material properties used in this study are listed in Table 7[10].

Table 7 Effective and total shear strengths [10]*.

Zone ID	Unit weight: kN/m3	Shear strength parameters				Geophysical data, Fig. 5(a)		Poisson's ratio, v
		Effective		Total				
		Cohesion, c: kPa	Angle of internal friction, φ'°	c: kPa	φ°	Shear wave velocity, Vs, m/s	Depth range, m	
Zone 1	20.88	11.35	24.0	8.95	15.2	365.8	0-6	
						426.8	> 6	
Zone 2 El. > 80m	21.35	7.09	25.0	2.15	16.3	365.8	0-6	0.25 for depth 0-24 m 0.30 for depth > 24m
						426.8	6-24	
Zone 2 El. < 180m	18.52	20.97	15.2	13.07	12.0	335.4 – 457.3	Linear increase from 24-64	
Zone 4	21.82	16.18	19.7	16.14	12.3	365.8	0-6	
						518.3	6 – 15	
						670.7	> 15	
Bedrock	23.56	47.88	45.0	47.88	45.0	914.4	all	

The shear strengths of the embankment materials are based on consolidated undrained triaxial test data; the stiffness values are based on geophysical test data. The corresponding values for bedrock are typical of sandstones and shales of the Franciscan Formation. Shear modulus G = mass density (ρ)×Vs2; Bulk modulus, K = 2(1+ v)/3(1-2 v)×G

For reduction in shear modulus and increase in damping during seismic loading, the shear modulus (G/G_{max}) and damping ratio (ξ) versus cyclic shear strain (γc) data for sand in [26] are used. Figures 5(b, c) shows plots of these data. The damping curve in Fig. 5(c) is the lowest of the three damping curves in [26]. Discrete values of the data used in Figs. 5(b, c) plots are listed in Table 8.

Table 8 Hysteretic characteristics: scaled values from [26] for sand

Hysteretic characteristics data for sands		Cyclic shear strain, γc, %										
		1×10^{-4}	3.16×0^{-4}	1×10^{-3}	3.16×0^{-3}	1×10^{-2}	3.16×10^{-2}	1×10^{-1}	3.16×10^{-1}	1	3.16	10
G/$Gmax$ curve	upper	1	1	0.99	0.95	0.85	0.64	0.37	0.18	0.09	0.04	0.01
	average	1	0.99	0.96	0.89	0.75	0.53	0.30	0.14	0.06	0.03	0.01
	lower	1	0.98	0.92	0.82	0.64	0.42	0.23	0.11	0.04	0.02	0.01
ξ, %	lower	0.24	0.42	0.73	1.39	2.73	5.21	9.82	15.70	21.21	24.0	24.0

3.1 Computer Programs Used

The computer programs used in this study are: SHAKEM[12] and FLAC[13]. SHAKEM is a modified version of the computer program SHAKE[14]; SHAKEM allows use of finite width of layers in the dam cross section whereas SHAKE uses infinite length of layers – both programs are for horizontally layered soil deposits overlying a rigid base (bedrock) subjected to a horizontal acceleration base motion. The solution scheme implemented in SHAKE is called equivalent linear as it accounts for nonlinearity of the shear modulus and damping via equivalent linear soil properties. FLAC allows use of different geometric configurations of soil deposits; linear elasticity, viscoelasticity, and plasticity-based nonlinear material models overlying a firm base with different stiffnesses subjected to one or two orthogonal components of acceleration (or velocity, force). The solution scheme implemented in FLAC is based on continuum-mechanics principles. For additional information, see the cited references for the two programs.

3.2 Numerical and Material Models Used

Figure 6 shows schematic descriptions of numerical models used in this study. Two planar sections were used to model the dam to assess the dam performance during the 1989 Loma Prieta earthquake – one section is located near Sta. 17+50; the other section is along the dam axis. Each section was used to calculate elastic vibration characteristics (frequencies and mode shapes) of the dam and identify tension zones associated with dam vibrations. In addition, each section was analyzed for permanent displacements at the dam crest and identification of tension zones. In summary, each section was analyzed for (a) acceleration and displacement response during the seismic excitation, and (b) permanent deformations, and location of tension zones at the end of the seismic excitation in continuum models. Continuum base analyses using FLAC were for plane strain conditions.
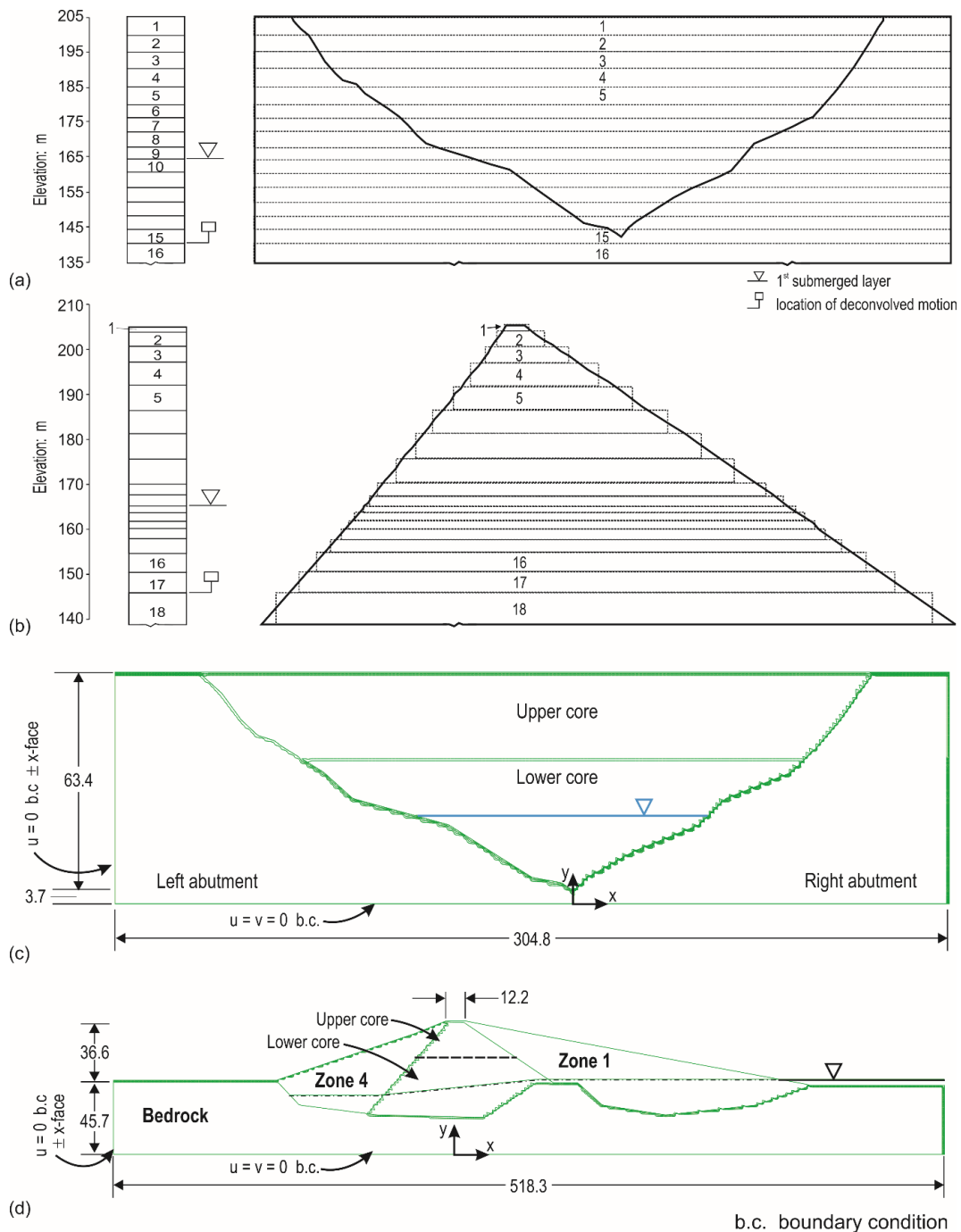
Figure 6. Schematic descriptions of numerical models of the Lexington Dam (Figs. 1b and 1c): (a) SHAKEM model for the longitudinal section; (b) SHAKEM model for the cross section; (c) FLAC model for the longitudinal section; (d) FLAC model for the cross section.

Three material models used are: (i) linear elastic; (ii) viscoelastic; and (iii) elastoplastic. Specifically, material model (ii) was used in SHAKEM for deconvolution of recorded accelerations at the left abutment to the base of the dam, and to calculate accelerations at top of the layers in the model; and material models (i), (ii) and (iii) were used in FLAC. Results from these analyses were compared with the accelerations records at the dam crest.

Plane stress vs plane strain conditions: Plane stress condition is considered appropriate for deformation analysis of thin structural members in which state of stress in the out-of-plane directions is negligible (e.g., thin plates, thin wall cylinders, amongst others). Plane strain condition is considered appropriate for analyses of long structures in which deformations in the out-of-plane directions are negligible (e.g., earth dams, tunnels, amongst other facilities).

In dam engineering practice, plane strain conditions are assumed in 2-D analyses of earth dams. Plane strain conditions were assumed in numerical analyses of the Lexington Dam.

However, for the longitudinal section of the dam, plane stress assumption was used because of limited extent of the out-of-plane dimension (crest width of 12 m). It suffices to say that for the linear elastic material model, the static and dynamic analysis results in terms of tension zones and deformations were similar to the ones with plane strain conditions; for viscoelastic material model, the results were different; and for the elastoplastic material model, the computer program FLAC did not allow use of plane stress setup.

3.3 Numerical Analyses Performed

Three sets of numerical analyses performed are for determination of: (i) natural vibration characteristics; deconvolution of recorded motions; and (iii) stresses and deformations. Items of particular interest in the numerical analyses are: (a) identification of tension zones; and (b) permanent displacements at the dam crest. Since the numerical methods used are based on continuum-mechanics principles, only the locations of tension zones are identified where cracks would be expected to occur. Details of numerical analyses performed are described in the following sections.

3.4 Natural Vibration Characteristics

Natural frequencies of vibration and associated mode shapes were calculated for the longitudinal and transverse and sections shown in Figs. 6(c, d). The procedure used is described in [27].   In brief, the procedure has two steps: the first step is to calculate natural frequencies, and the second step is to calculate the mode shapes associated with the natural frequencies. This procedure was implemented in FLAC models of the transverse and longitudinal sections.

For the natural frequencies, a dynamic analysis of elastic model was performed for 20 s; the dynamic excitation was a horizontal force of 4.5 kN magnitude varying in the form of a high frequency (100 Hz) and short duration (0.01 s) sine pulse applied evenly among the nodes at the dam crest. Displacements in the x- and y- (horizontal and vertical) direction at select locations along the dam height were saved at 10 steps interval (about 0.003 s). At the end of the dynamic analysis, an FFT analysis of the displacement-time histories were performed, and the results plotted which are in the form of frequency (abscissa) and Fourier amplitude (ordinate); spikes in the plots of the FFT analysis results correspond to the natural frequencies of the dam, and the frequency corresponding to the 1st spike is taken to represent the fundamental frequency of the dam-foundation-reservoir system modeled.

For the mode shapes, a dynamic analysis of the model was performed for 20 s; the dynamic excitation was a horizontal force of 4.5 kN magnitude varying in the form of a continuous sine wave of desired frequency, f, and 20 s duration applied evenly among the nodes at the dam crest. Displacements in the x- and y- directions at select location along the height of the dam were saved at 10 steps interval (about 0.003 s). At the end of the dynamic analysis, the plot of the deformed grid is the mode shape associated with the frequency, f, that was used to generate the continuous sine wave.

Longitudinal section results: The x-direction in the longitudinal section is in the dam-axis direction and the y-direction is vertical. The results for the longitudinal section are shown in Fig. 7. The spikes in the FFT of the displacement-time history at the dam crest in the x-direction occur at frequencies: 2.40, 3.60, 6.05, 6.60,

8.70, ... Hz; the corresponding spikes in the FFT of the displacement history in the y-direction occur at frequency: 3.20, 3.60, 5.10, 5.70, 6.15, … Hz. The mode shape plots for the 1st natural frequency f1 = 2.4 Hz in the horizontal and 3.2 Hz in the vertical direction are shown in Figs. 7(e, f), respectively. Contour lines which separate regions of tension and compression (tension contour) are shown for each of the mode shape plots – tension contour is the zero contour for the effective minor principal stresses in the model. Similar plots for mode shapes associated with higher frequencies were developed and tension zones identified. These are not included herein to conserve space.
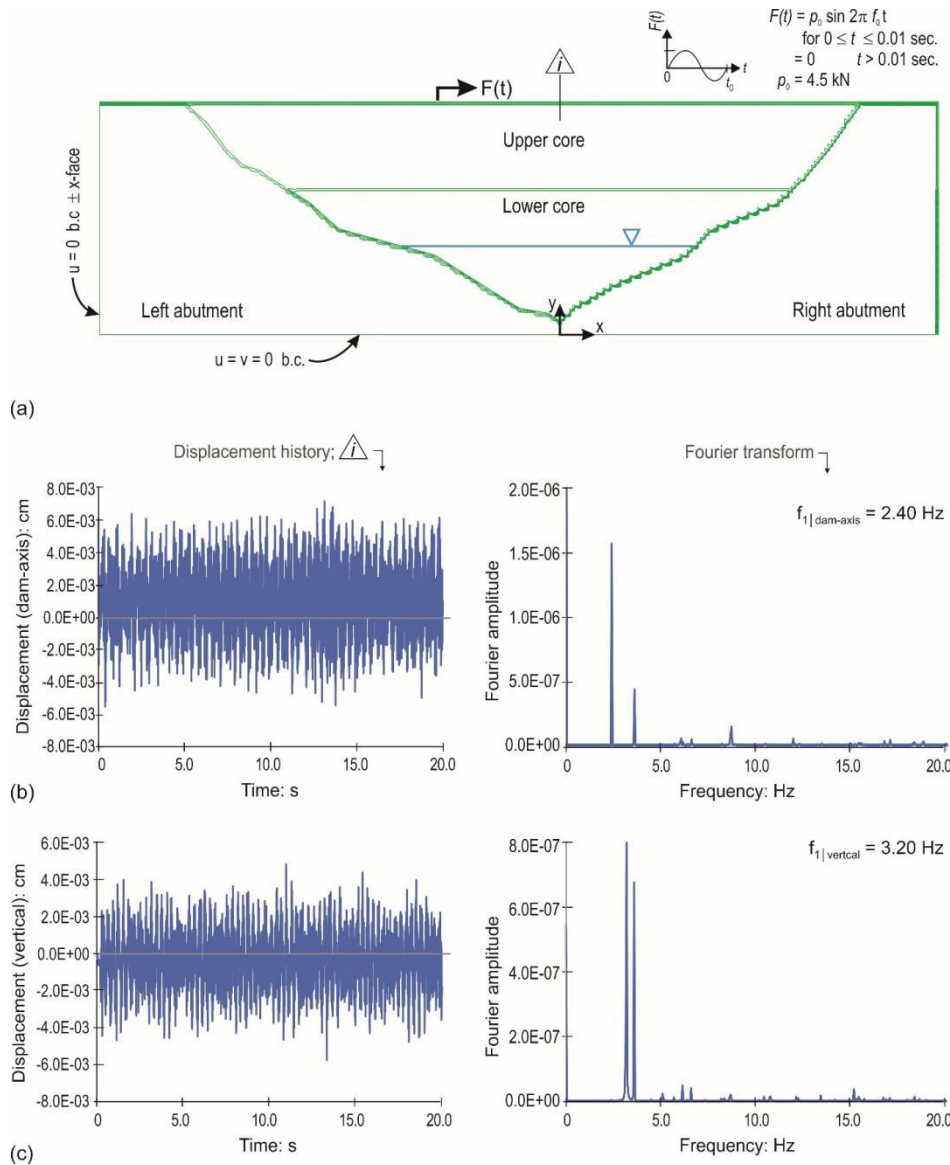
Figure 7. Computed natural vibration frequencies and mode shapes of the dam in longitudinal direction: (a) model setup for frequency analysis; (b) longitudinal vibration frequencies; (c) vertical vibration frequencies; (d) model setup for mode shape analysis; (e) 1st mode shape in the longitudinal direction; (f) 1st mode shape in the vertical direction.

Transverse section results: The x-direction in the transverse section is in the u/s-d/s direction and the y-direction is vertical. The results for the transverse section are shown in Fig. 8. The spikes in the FFT of the displacement-time history at the dam crest in the x-directions occur at frequencies: 2.45, 3.10, 3.45, ... Hz; the corresponding spikes in the y-direction FFT occur at frequencies: 2.45, 3.10, 3.90, … Hz. The mode shape plots for f = 2.45, and 3.10 shown in Figs. 8(e, f) are the deformed shapes of the grid. A contour which separates regions of tension and compression is shown for each of the mode shape plots – the tension contour is the zero contour for the effective minor principal stresses in the model.

Tension regions identified on the mode shape plots in Figs. 7(e, f) and 8 (e, f) provide sharply demarcated

regions near the dam-abutment contacts and on the u/s and d/s dam faces, and in the interior of the dam where cracks would be expected, if they were to occur, under existing and/or seismic loadings. The visible cracks and their depths identified in the post-seismic inspections and investigations of the dam site are well within the bounds of the demarcated regions labeled as tension zones in Figs. 7 and 8 (e, f); see Fig. 2(f) for the observed locations of cracks, and for the depth of observed cracks, see the Dam cracks section . Computed values of the 1st and 2nd natural frequencies of the dam in each of the three references directions are summarized in Table 9.

Table 9   Computed resonant frequencies for the Lexington Dam.

Dam reference direction	Computed resonant frequency): Hz	
	f1	f2
Longitudinal	2.4	3.6
Transverse	2.45	3.45
Vertical	3.2/3.1	3.6
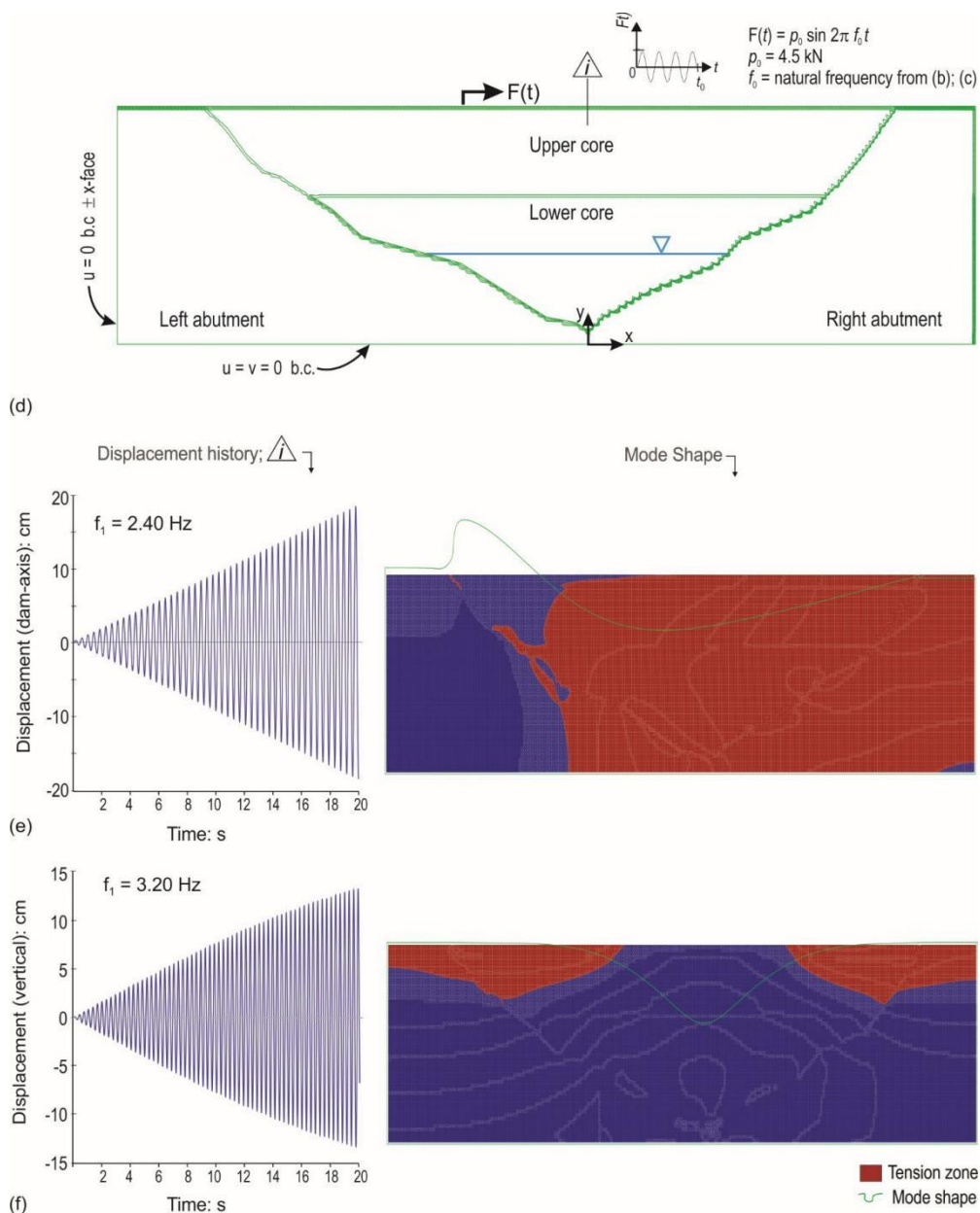
Figure 7.   (Continued.)

Significant observation on natural vibrations results:

(1) The computed natural vibration frequency in the vertical direction from two independent sections (longitudinal and transverse) is essentially identical (3.2 vs 3.1 H).

(2) Comparisons of tension zones identified in mode shape plots with the observed crack locations show agreement between the model results and observations.

(3) The model results also point out tension zones which are located at depth in the interior of the dam. However, the post seismic inspection of the dam were limited to the surface observations.
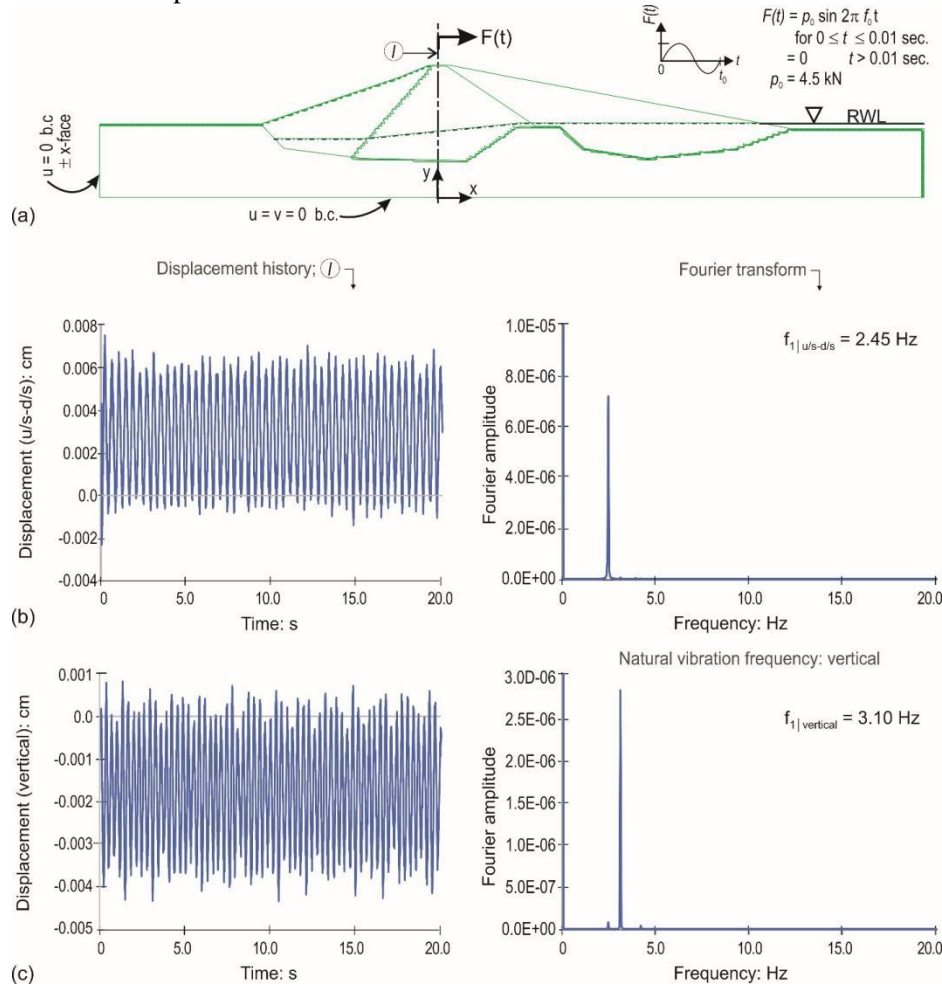
Figure 8. Computed natural vibration frequencies and mode shapes of the dam in transverse direction: (a) model setup for frequency analysis; (b) transverse vibration frequencies; (c) vertical vibration frequencies; (d) model setup for mode shape analysis; (e) 1st mode shape in the transverse direction; (f) 1st mode shape in the vertical direction.

4. Deconvolution of Motions Recorded at the Left Abutment

There was no strong motion instrument located near the dam base. The left abutment accelerometer data were deconvolved to the base of the dam using the 1-D wave propagation procedure described in this section.

Equivalent linear material model with hysteretic stress-strain characteristics of frictional soils was used for deconvolution of the left abutment CH1 and CH3 accelerations data to the base of the dam. One-dimensional (1-D) representations of the longitudinal and transverse sections shown in Figs. 6(a) and 6(b) were used for this purpose. The solution scheme for the analysis is described in [14] and [12]. Width of the dam in transverse section and length of the model in the longitudinal direction were included in the calculations via SHAKEM input data for the respective sections. The uniform shear strain was set to be $0.59 \times$ maximum shear strain; the 0.59 factor is based on the relation: $(M-1)/10$[28]. For the 1989 Loma Prieta seismic event, M = 6.9. The CH1 and CH3 recorded motions were treated as rock outcrop motions. The computed results are for: (i) acceleration-time

series at the top of bedrock and at crest of the dam, and (ii) maximum accelerations, cyclic shear stresses and strains along the height of the SHAKEM columns. The analysis results for each of the two models are described below.

Longitudinal section results: The 1-D SHAKEM column is divided in 16 layers – the 16th layer is the half-space (bedrock). Figure 9(a) shows the variations in maximum acceleration at the top of each of the sixteen layers along the height of the dam near the center of the valley. The computed maximum accelerations at the dam crest are: 0.28g; 0.35g; 0.41g for the lower, average, and upper G/G_{max} curves, respectively; see Fig. 5(b) for the G/G_{max} curves. The corresponding maximum acceleration values in the deconvolved motions at the base of the dam are 0.37g; 0.38g; and 0.37g. For reference, these results are shown in Table 10; maximum accelerations in the recorded data at the dam crest are also included in Table 10.
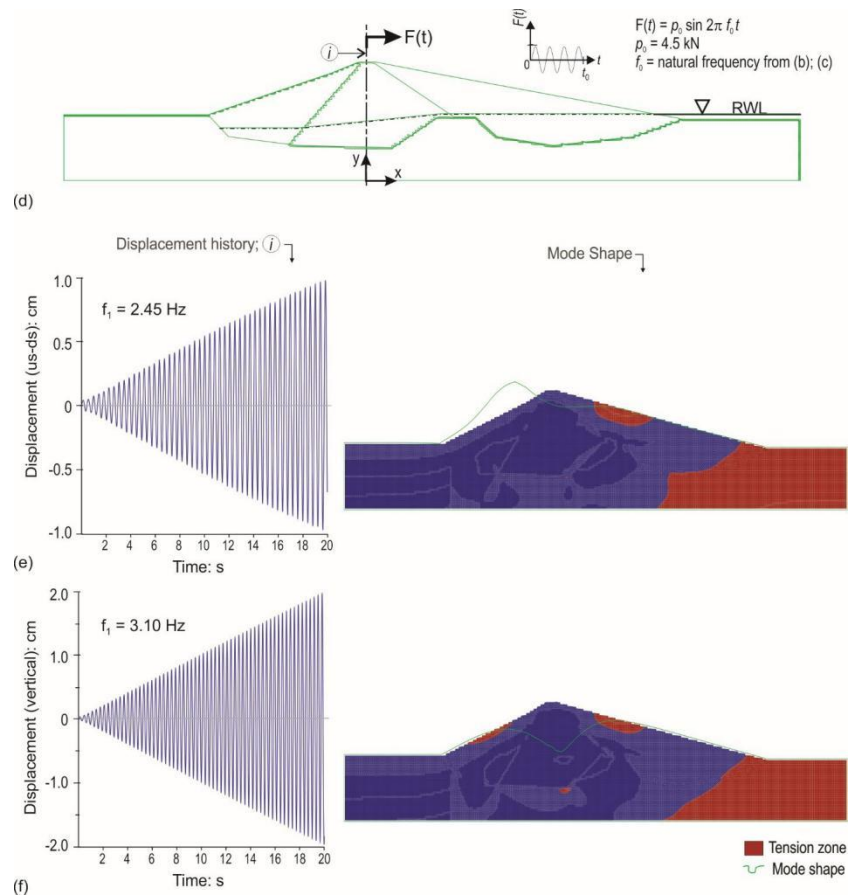
Figure 8.   (Continued.)

Table 10   Peak ground accelerations in computed and recorded motions at dam crest; 1-D model, longitudinal section.

Location ID	Peak ground acceleration in the dam-axis direction: g					
	Computed			Measured		
	G/G_{max} curve			Instrument location		
	lower	average	upper	Left crest	Right crest	Left abutment
Layer 1 (dam crest)	0.28	0.35	0.41	0.39	0.33	0.41
Layer 16 (inlayer) (dam-foundation contact)	0.37	0.38	0.37	-	-	-
AFC*	0.76	0.92	1.11			

AFC = acceleration amplification factor; AFC = Peak crest acceleration / Peak ground acceleration

An assessment of the maximum strain plots in Fig. 9(a) shows that use of lower G/G_{max} curve results in shear stains > 1% in the middle 3rd of the dam height which is considered unacceptable because G/G_{max} data for

strain > 1% are not based on laboratory tests – it was created to avoid numerical problems associated with lack of data. Use of the upper G/G_{max} curve data was considered most appropriate for the longitudinal section based on the rationale that: (i) the dam is relatively more constrained in the longitudinal direction than it is in the transverse direction – displacements and strains in longitudinal direction will be expected to remain smaller than their counterparts in transverse direction; (ii) smaller cyclic strains require smaller reduction of shear modulus from its initial G_{max} value; (iii) computed maximum shear stresses are considered reasonable in view of (i), (ii), and the G/G_{max} data plots shown in Fig. 5(b); and (iv) variations in computed maximum shear strain along the height of the dam and their magnitudes are more like the ones observed in past studies of other dams. The upper G/G_{max} curve represents the least reduction in shear modulus during cyclic loading and its use leads to the computed maximum shear strains well within the range of measured data. Computed results from use of the upper G/G_{max} curve are shown below:

The time-acceleration histories of the computed motions at the dam base and dam crest are shown in Figure 9(b); FFTs of these motions are shown in Fig. 9(c); and Fourier amplifications of computed motions at the dam crest are shown in Fig. 9(d). The Fourier amplifications are obtained by dividing the FFT of the crest motion by the FFT of the base motion.
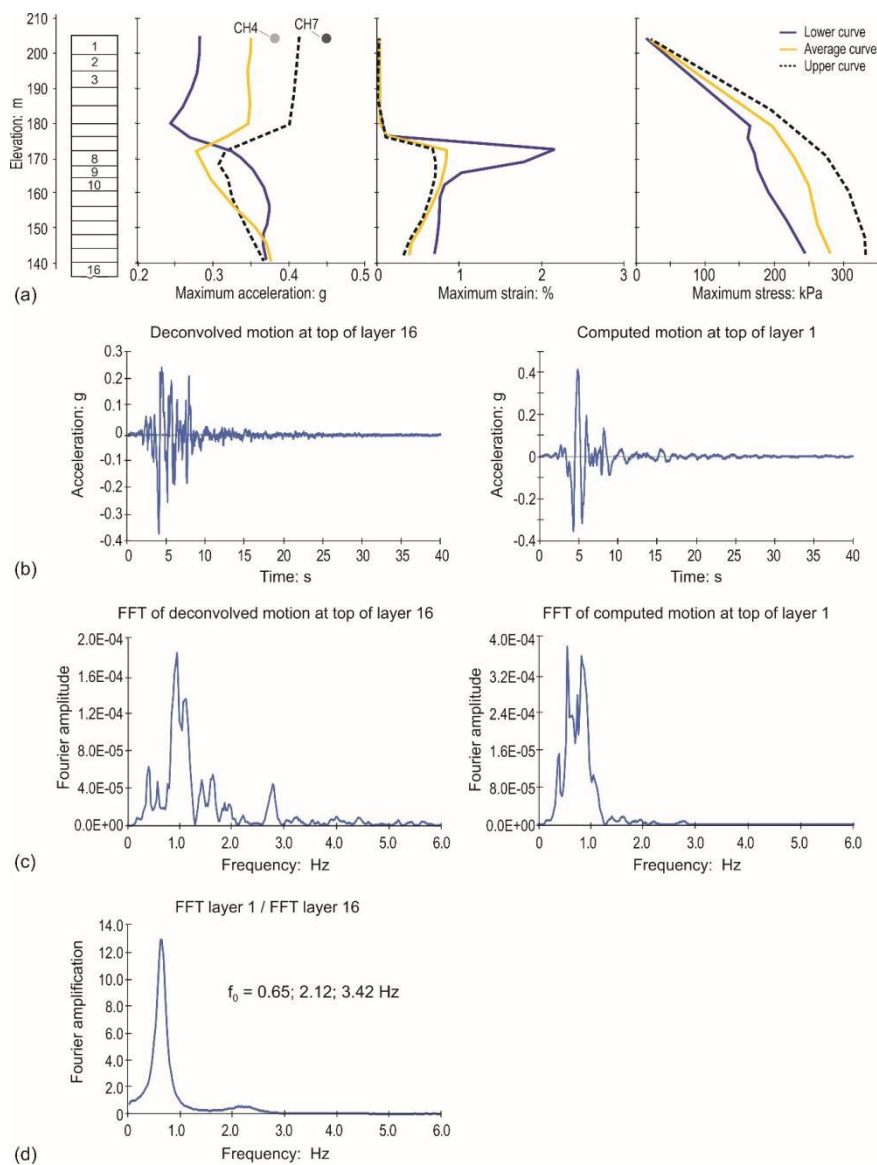
Figure 9. SHAKEM model results for the longitudinal section: (a) maximum acceleration, shear strain, and shear stress along the dam height near Stn. 17+50; (b) computed motion at the top of the bedrock, and the dam crest in the dam-axis direction; (c) Fourier transforms of computed motions in (b); (d) Fourier amplification spectrum using the FFTs in (c); (cont.).

Figure 9(d) graph suggest the resonant frequencies of the dam are about 0.65 Hz and 2.12 Hz. A mode shape analysis for 0.65 Hz sine wave did not create a mode shape and the displacement pattern expected of a resonant frequency – therefore it was dropped from further considerations. The tabulated values of the Fourier amplification spectrum were examined for a frequency associated with the next spike and found it to be 3.42 Hz. The 2.12 Hz sine wave creates a mode shape similar to the one for the 2.4 Hz frequency in the dam axis direction (Fig. 7e); the displacement pattern has 5.5 beats in the 20 s of dynamic time – this gives a beat frequency of 0.275 Hz (5.5/20). Thus, the resonant frequency is 2.12+0.275 = 2.395 (~2.40 Hz). Similarly, the 3.42 Hz frequency sine wave creates a mode shape which is similar to the one for 3.20 Hz frequency in the vertical direction (Fig. 7f); the displacement pattern has 4.5 beats in the 20 s of dynamic time – this gives a beat frequency of 0.225 Hz (4.5/20). Thus, the resonant frequency in the vertical direction is 3.42–0.225 = 3.195 Hz (~3.20 Hz). The computed displacement patterns and mode shape plots for the 2.12 Hz and 3.20 Hz sine waves are shown in Figs. 9(c) and 9(f), respectively.

For comparison, overlays of the computed motion at the dam crest, in the dam-axis direction, and the CH4 and CH7 recorded accelerations are shown in Fig. 9(g); and the overlays of their FFTs are shown in Fig. 9(h). These plots show a reasonable agreement between the computed and measured values.
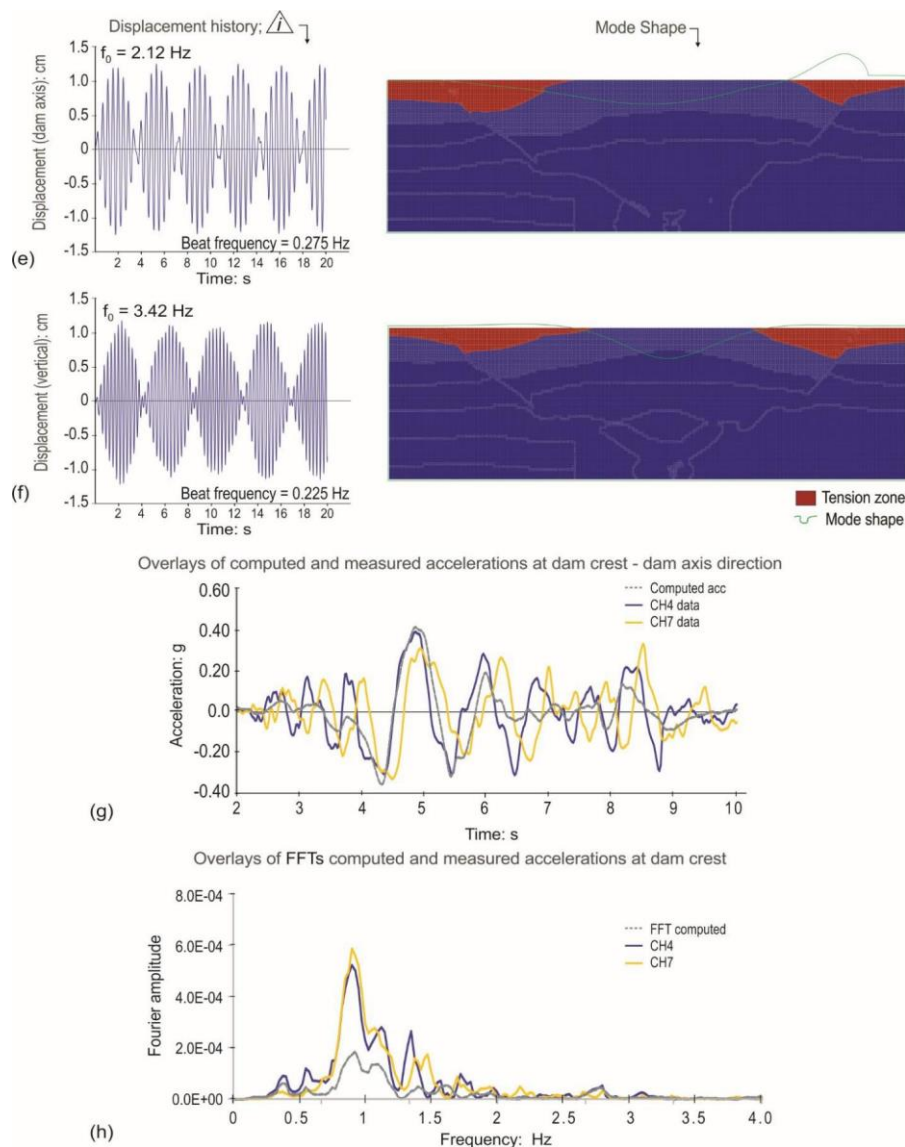
Figure 9.   (Continued)

Transverse section results: Figure 10(a) shows maximum computed acceleration at the top of each of the eighteen layers along the centerline of the dam. The computed maximum accelerations at the crest of the dam are: 0.43g; 0.57g; 0.63g for the lower; average; and upper G/G_{max} curves shown in Fig. 5. The corresponding computed maximum acceleration values in the deconvolved motions at the base of the dam are 0.42g; 0.42g; and 0.41g. For quick reference, these results are shown in Table 11; maximum accelerations in the recorded data are also included in Table 11.

Table 11 Peak ground accelerations in computed and recorded motions; transverse section; 1-D model.

Location	Peak ground acceleration – u/s-d/s direction: g					
	Computed			Measured		
	G/G_{max} curve			Instrument location		
	lower	average	upper	Left crest	Right crest	Left abutment
Stn. 17+50	0.43	0.57	0.63	0.38	0.45	0.44
Base	0.42	0.42	0.41	-		
AFC*	1.02	1.36	1.54			

* AFC = acceleration amplification factor; AFC = Peak crest acceleration / Peak ground acceleration

An assessment of the maximum strain plots in Fig. 10(a) shows that use of lower G/G_{max} curve results in shear stains > 1% in the middle 3rd of the dam height which is considered unacceptable because G/G_{max} data for strain > 1% are not based on laboratory tests – it were created to avoid numerical problems associated with lack of data. Use of the average G/G_{max} curve data was considered most appropriate for the transverse section based on the rationale: (i) the dam is relatively less constrained in the transverse direction than it is in the longitudinal direction – displacements and strains in transverse direction will be expected to remain larger than their counterparts in longitudinal direction; (ii) larger cyclic strains require larger reduction of shear modulus from its initial G_{max} value; (iii) computed maximum shear stresses are considered reasonable in view of (i), (ii), and the G/G_{max} data plots shown in Fig. 5(b); and (iv) variations in computed maximum shear strain along the height of the dam and their magnitudes are more like the ones observed in past studies of other dams. The average G/G_{max} curve represents the average reduction in shear modulus during cyclic loading and its use leads to the computed maximum shear strains well within the range of measured data. Computed results from use of average G/G_{max} curve are shown below:

The time-acceleration histories of the computed motions at the dam base and dam crest near Stn. 17+50 are shown in Fig. 10(b); FFTs of these motions are shown in Fig. 10(c); and Fourier amplifications of computed motions at the dam crest are shown in Fig. 10(d). The Fourier amplifications are obtained by dividing the FFT of the crest motion by the FFT of the base motion.

Figure 10(d) graph suggest the resonant frequencies of the dam are about 0.65 Hz and 1.80 Hz. A mode shape analysis for 0.65 Hz and 1.80 Hz sine waves did not create mode shapes and the displacement patterns expected of a resonant frequency – therefore these were dropped from further considerations. The next spike is associated with a frequency of 3.07 Hz. A 3.07 Hz frequency sine wave creates a mode shape similar to the one associated with 3.10 Hz frequency in the vertical direction (Fig. 8f); the displacement pattern has one beat in about 28 s of dynamic time – this gives a beat frequency of 0.036 Hz (1/28). Thus, the resonant frequency in the vertical direction is 3.07+0.036 = 3.106 Hz (~3.10 Hz). The computed displacement pattern and mode shape for the 3.07 Hz frequency sine wave are shown in Fig. 10(f). For illustration, displacement pattern and a mode shape for a stray frequency sine wave (of non-resonant frequency), the results for the 0.65 Hz sine wave are shown in Fig. 10(e).

For comparison, overlays of the computed motion at the dam crest, in the dam-axis direction, and the CH6 and CH9 recorded accelerations are shown in Fig. 10(g); and the overlays of their FFTs are shown in Fig. 10(h).
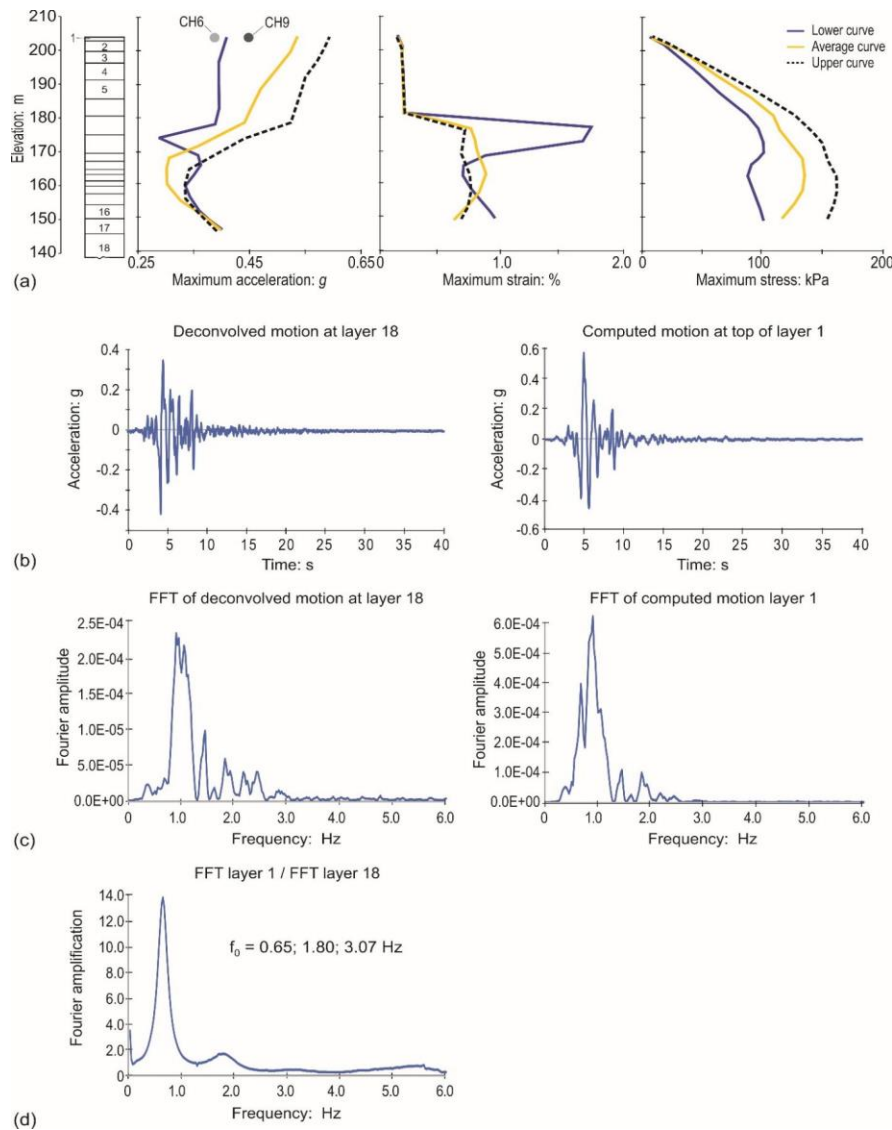
Figure 10. SHAKEM model results for the transverse section: (a) maximum acceleration, shear strain, and shear stress along the dam centerline; (b) computed motion at the top of the bedrock, and the dam crest in the u/s-d/s direction; (c) Fourier transforms of computed motions in (b); (d) Fourier amplification spectrum using the FFTs in (c); (e) mode shape associated with computed frequency in transverse direction; (f) mode shape associated with computed frequency in vertical direction; (g) overlays of computed motion at the dam crest and the recorded CH6 and CH9 data; (h) overlays of FFTs of motions in (g). Plots in (b) to (h) are from use of the average curve in (a).

These plots show a reasonable agreement between the computed and measured values.

Inverse analyses using SHAKEM models: The SHAKEM columns for the longitudinal and transverse sections were analyzed using the deconvolved motion as an inlayer motion in the respective sections. In these analyses the outcrop motion for the base rock was determined as part of the output. The resulting outcrop motions were identical to the left abutment motions. This information was considered as a confirmation of the correctness of the deconvolved motions.

Significant observations on deconvolution analyses results:

(1) The maximum acceleration values in the deconvolved motions in the dam-axis, and u/s-d/s directions for the three G/G_{max} curves data are about the same; the small difference of 0.01g can be ignored due to numerical arithmetic.
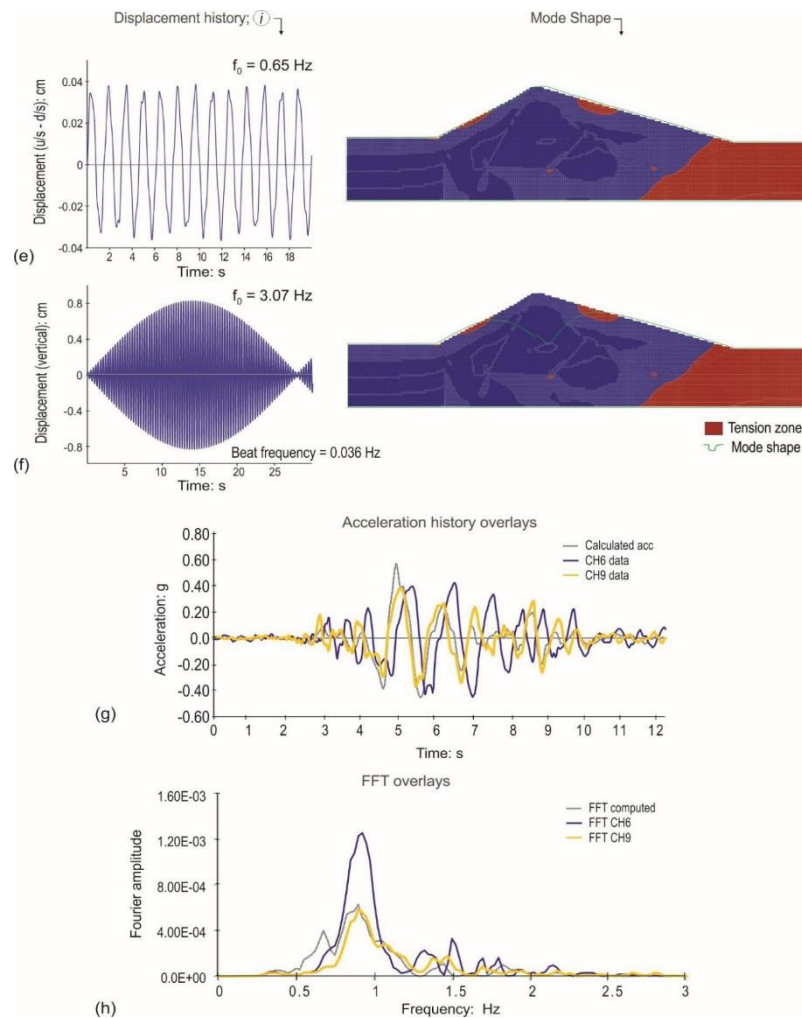
Figure 10.   (Continued)

(2) The computed maximum accelerations at the dam crest in the longitudinal (dam-axis) and transverse (u/s-d/s) directions compare reasonably well with the recorded counterparts considering the use of published G/G_{max} data because of lack of actual soil test data for the Lexington Dam materials.

(3) The overlays of computed and recorded time acceleration data and their FFTs shown in Figs. 9(c, d) and 10(c, d) are considered good for reasons given in observation (2).

(4) Computed maximum acceleration plots in Fig. 10(a) show increasing amplifications of accelerations in the u/s-d/s direction in the upper half of the dam height; it is a typical response of well-compacted earth dams under strong shaking, and is known as whiplash phenomena[3]. This phenomenon is not present in the corresponding plots in Fig. 9(a) for the longitudinal section.

(5) The amplification factor (AFC) values listed in Tables 10 and 11 are of similar magnitude as compared to the ones based on actual measured data on other dams[1,3].

(6) The frequency results based on the Fourier amplification spectrum are essentially identical to the ones calculated independently via natural vibration calculation procedure. It is recognized that the frequencies determined via Fourier amplification spectrum shown in Figs. 9(d) and 10(d) create beats in the displacement response; however, the beat frequency can be used to correct for the effects of finite number of layers used in the SHAKEM column.

The deconvolved motions shown in Figs. 9(b) and 10(b) were used as base motions for the deformation analyses using the computer program FLAC as described in the next section.

5. Deformation Analyses

The longitudinal and transverse sections shown in Fig. 6 were used for deformation analyses. The material properties used for analyses are shown in Tables 7 and 8 and Fig. 5b. The three material models used were: (i) linear elastic; (ii) viscoelastic; and (iii) elastoplastic with Mohr-Coulomb yield criterion. The deconvolved time-acceleration histories in the longitudinal and transverse directions were used for seismic excitations of the numerical models. The dam loads were applied in one lift; pore pressure conditions were for the low reservoir water level (RWL = 168.4 m) and a low phreatic surface, [10]; dynamic excitations were via use of acceleration-time series. Dynamic analyses were performed in continuation to the static analyses.

For the static analyses, the standard procedure in FLAC with material properties required for the material model selected, were used. For dynamic analysis using linear elastic material model, 5 percent of critical damping was used; for the viscoelastic material model, hysteretic damping with Hardin and Drnevich reference strain value at 50 percent of G/G_{max} was used; and for the elastoplastic material model, implicit damping associated with cyclic loading-unloading-reloading and plastic flow was used. For details on damping options and their implementations in FLAC, see software documentations in [13]. Results from analysis of the two planar sections are described in the following two subsections.

5.1 Longitudinal section results

Figure 11 shows the continuum-based results for the static and dynamic loads for the three material models used. Figure 11(a) shows the model setup for the longitudinal section of the dam along the dam center line; the boundary conditions for dynamic analysis are shown on Fig. 11(a); the boundary conditions for static analyses are shown on Fig. 6(c). For ease of comparison, static and dynamic analyses results for linear elastic, equivalent linear, and elastoplastic material models are shown using three column format; the columns are marked with the header 'Linear elastic', 'Viscoelastic', and 'elastoplastic'.

Locations of tension zones for the three material models in static and dynamic analysis results are shown in rows (b) and (c), respectively. Linear elastic material model results show tension zones near the left and right abutments for static and dynamic loads; the tension zones are essentially at the same locations and of about the same size. The viscoelastic material model results show tension zones in the static and dynamic analyses results. Elastoplastic material model results show no tension zones for static and dynamic loads. These results are shown in rows marked (b), and (c). The field data show tension cracks near the abutments – dam stations 13+00 and 21+10, see Fig. 2(f).

Variations in maximum accelerations along the dam height are shown in the row (d); the recorded peak accelerations at the dam crest in the dam-axis direction (Channel 4 and Channel 7) are included for comparison. The computed maximum acceleration at the dam crest is about 1.67 g in linear elastic model, about 1.03 g in viscoelastic; and about 0.52 g in elastoplastic material model. The corresponding peak accelerations in recorded motions are: 0.3917 g (CH4) and 0.3340 g (CH7)

The computed motion at the dam crest; the FFTs of computed motion at the dam crest and the deconvolved input base motion applied; and the Fourier amplification spectrum of the computed motion and input motion are shown in rows (e), (f), (g), and (h), respectively. There are differences in the computed time-acceleration histories and their FFTs for the linear elastic, viscoelastic, and elastoplastic material models to the same applied input motion shown in Fig. 11(a). The Fourier amplification graphs shown in row (h) were obtained by dividing the FFT of computed motions shown in row (f) with the FFT of input motion shown in row (g). The peaks in Fourier amplification: for the linear elastic material model occur at frequency 2.25, 2.4, 2.45, 2.62, 3.0, … Hz; for the viscoelastic material model occur at frequency 2.0, 2.3, 2.5, 3.4, 3.8, … Hz; and for the elastoplastic material model at frequency 2.0, 2.12, 2.25, 2.37, 2.42, … Hz. For ease of reference these values are tabulated in Table 12. No mode shape analyses were performed to validate their being resonant frequency or a stray frequency wave; and they are compared by their numerical value alone with the calculated 1st resonant frequency in the

three coordinate directions.
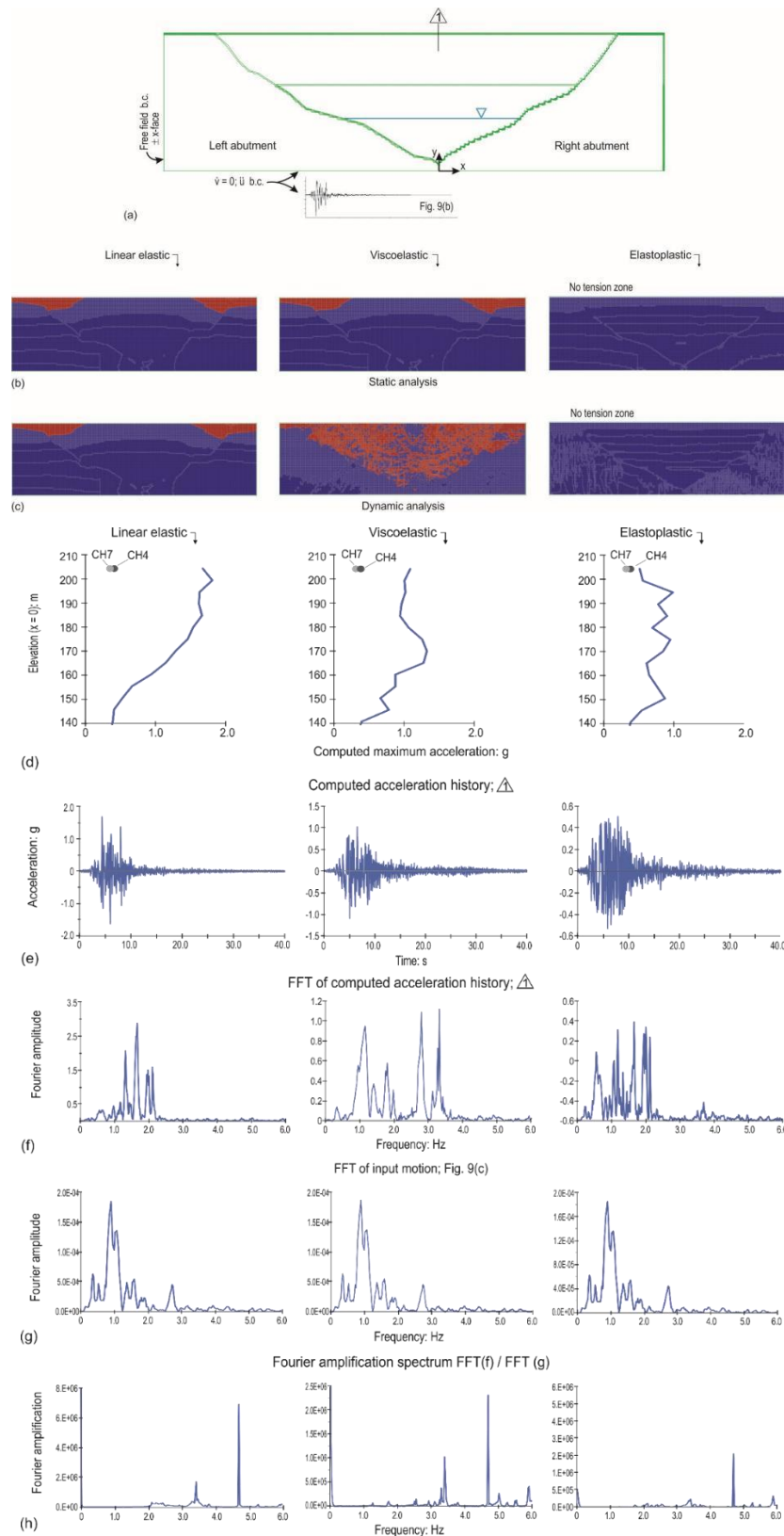
Figure 11. Details of the computed FLAC model results for the longitudinal section using linear elastic, viscoelastic, and elastoplastic material models: (a) model setup; (b) tension zones based on static analysis; (c) tension zones based on dynamic analysis; (d) maximum acceleration along the ; (e) time-acceleration history at the dam crest; (f) FFT of computed motion in (e); (g) FFT of dynamic excitation motion shown in (a); (h) Fourier amplification spectrum using FFTs in (f) and (g); (i) overlays of computed and recoded accelerations

at the dam crest; (j) overlays of FFTs of motions in (i); (k) overlays of computed and measured settlements at the dam crest (distance 0 is at Sta. 13+00).
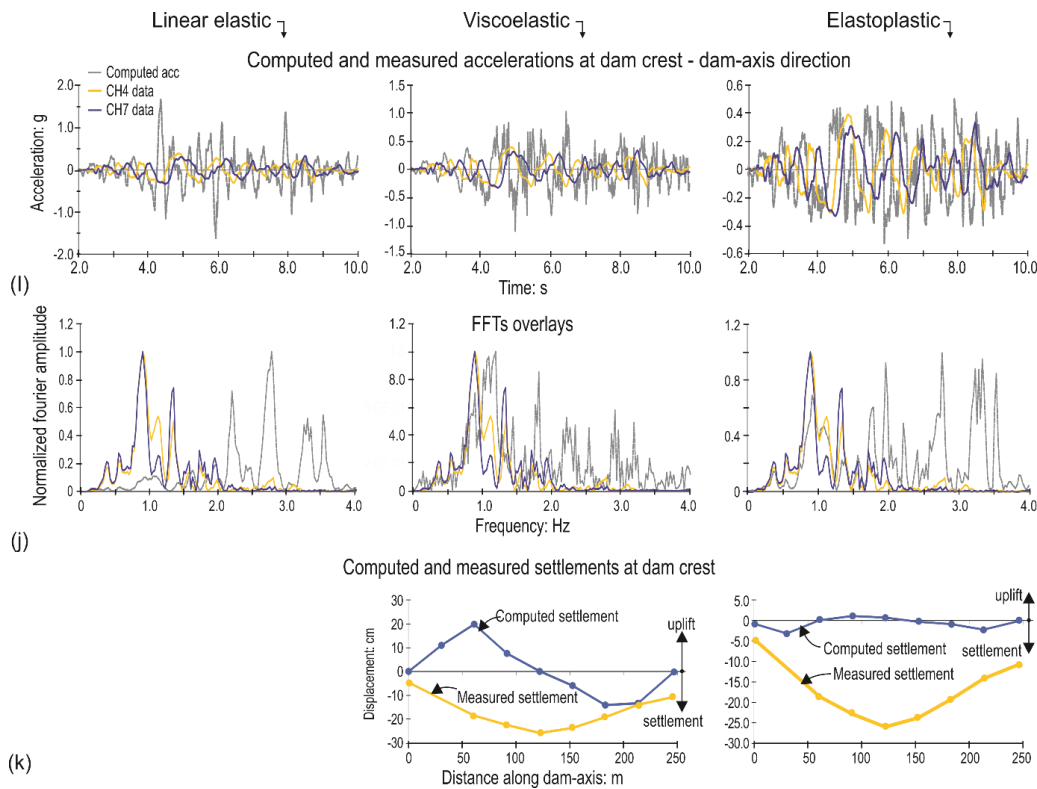
Figure 11. (Continued)

The overlays of computed motions and the recorded motions at the dam crest (CH4 and CH7) are shown in row (i) and the overlays of their FFTs (normalized to a Fourier amplitude of 1.0) are shown in row (j). By appearance, the FFTs for viscoelastic and elastoplastic material models compare better than for the linear elastic material model; however, computed results from all three material models compare poorly with their measured counterparts.

There are no computed permanent displacements for elastic material model; the computed permanent vertical (y-) displacements for the equivalent linear and elastoplastic material models are shown in row (k); the negative values imply settlements, and the positive values imply uplift. The measured settlements data are included in (k). Obviously, the computed settlements are much different than their measured counterparts. The graphs in Fig. 11(k) are interpreted to say that surface cracks on the dam crest shall be expected to occur near Stn. 15+00, 17+00, and 18+00 (the inflection points in Fig. 11(k) graphs). The observed surface cracks were on the u/s slope near Stn. 15+50 and 17+00; on d/s slope between stn. 17+50 and 18+00; and on the dam crest near Stns. 13+00 and 21+10, see Fig. 2(f).

Table 12 Frequencies correspond to the spikes in the Fourier amplification spectrum plots,

Fig. 11(h) – Longitudinal section, continuum-based analyses

Material model	Frequency: Hz				
	f (p1)	f (p2)	f (p3)	f (p4)	f (p5)
Linear elastic	2.25	2.4	2.45	2.62	3.0
viscoelastic	2.0	2.3	2.57	3.42	3.82
Elastoplastic	2.0	2.12	2.25	2.37	2.42
1st Resonant frequency (Linear elastic)	2.40(dam-axis)	2.45(u/s-d/s)	3.2(vert)		

5.2 Transverse section results

Figure 12 shows the continuum-based results for the static and dynamic loads for the three material models used. Figure 12(a) shows the model setup for the transverse section of the dam near Stn. 17+50; the boundary conditions for dynamic analysis are shown on Fig. 12(a); the boundary conditions for static analyses are shown on Fig. 6(d). For ease of comparison, static and dynamic analyses results for linear elastic, viscoelastic, and elastoplastic material models are shown using three column format; the columns are marked with the header 'Linear elastic', 'viscoelastic', and 'elastoplastic'.

Locations of tension zones for the three material models in static and dynamic analysis results are shown in rows (b) and (c), respectively. Linear elastic material model results show tension zones on the u/s and d/s faces of the dam for static and dynamic loads; the tension zones are essentially at the same locations and of about the same size. The viscoelastic material model results show tension zones in the static and dynamic analyses results. The elastoplastic material model results show no tension zones in the static analysis, and a small tension zone on the d/s face near the dam toe. These results are shown in rows marked (b), (c). The field data show cracks on the d/s slope of the dam near Stn. 17+50, see Fig. 2(f).
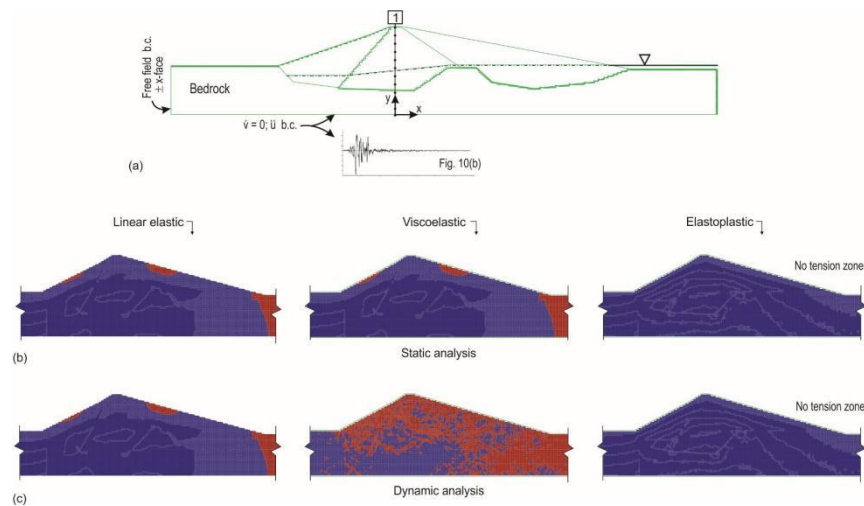
Figure 12. Details of the computed FLAC model results for the transverse section using linear elastic, viscoelastic, and elastoplastic material models: (a) model setup; (b) tension zones based on static analysis; (c) tension zones based on dynamic analysis; (d) maximum acceleration along the dam height near station 17+50; (e) time-acceleration history at the dam crest; (f) FFT of computed motion in (e); (g) FFT of dynamic excitation motion shown in (a); (h) Fourier amplification spectrum using FFTs in (f) and (g); (i) overlays of computed and recoded accelerations at the dam crest; (j) overlays of FFTs of motions in (i); (k) variations of transverse displacements along the dam centerline and its measured counterpart at the dam crest.

Variations in maximum accelerations along the dam height are shown in row (d); the recorded peak accelerations at the dam crest in the u/s-d/s direction (Channel 6 and Channel 9) are included for comparison. The computed maximum acceleration at the dam crest is about 1.95 g in linear elastic model, about 1.66g in viscoelastic, and about 0.52 g in elastoplastic model. The corresponding peak accelerations in recorded motions are: 0.3823 g (CH6) and 0.4502 g (CH9).

The computed motion at the dam crest; the FFTs of computed motion at the dam crest and the deconvolved input base motion applied; and the Fourier amplification spectrum of the computed motion and input motion are shown in rows (e), (f), (g), and (h), respectively. There are significant differences in the computed motions and their FFTs for the linear elastic, viscoelastic, and elastoplastic material models to the same applied input motion shown in Fig. 12(a). The Fourier amplification graphs shown in row (h) were obtained by dividing the FFT of computed motions shown in (f) with the FFT of input motion shown in (g). The peaks in Fourier amplification: for the linear elastic material model occur at frequency 1.32, 2.42, 2.65, 2.92, 3.17, … Hz; for the viscoelastic material model at frequency 1.30, 2.0, 2.30, 2.60, 3.15, … Hz; and for the elastoplastic material model at frequency 1.30, 1.55, 1.80, 1.87, 2.02, … Hz. For ease of reference these values are tabulated in Table 13. No

mode shape analyses were performed to validate their being resonant frequency or a stray frequency wave; and they are compared by their numerical value alone with the calculated 1st resonant frequency in the three coordinate directions.
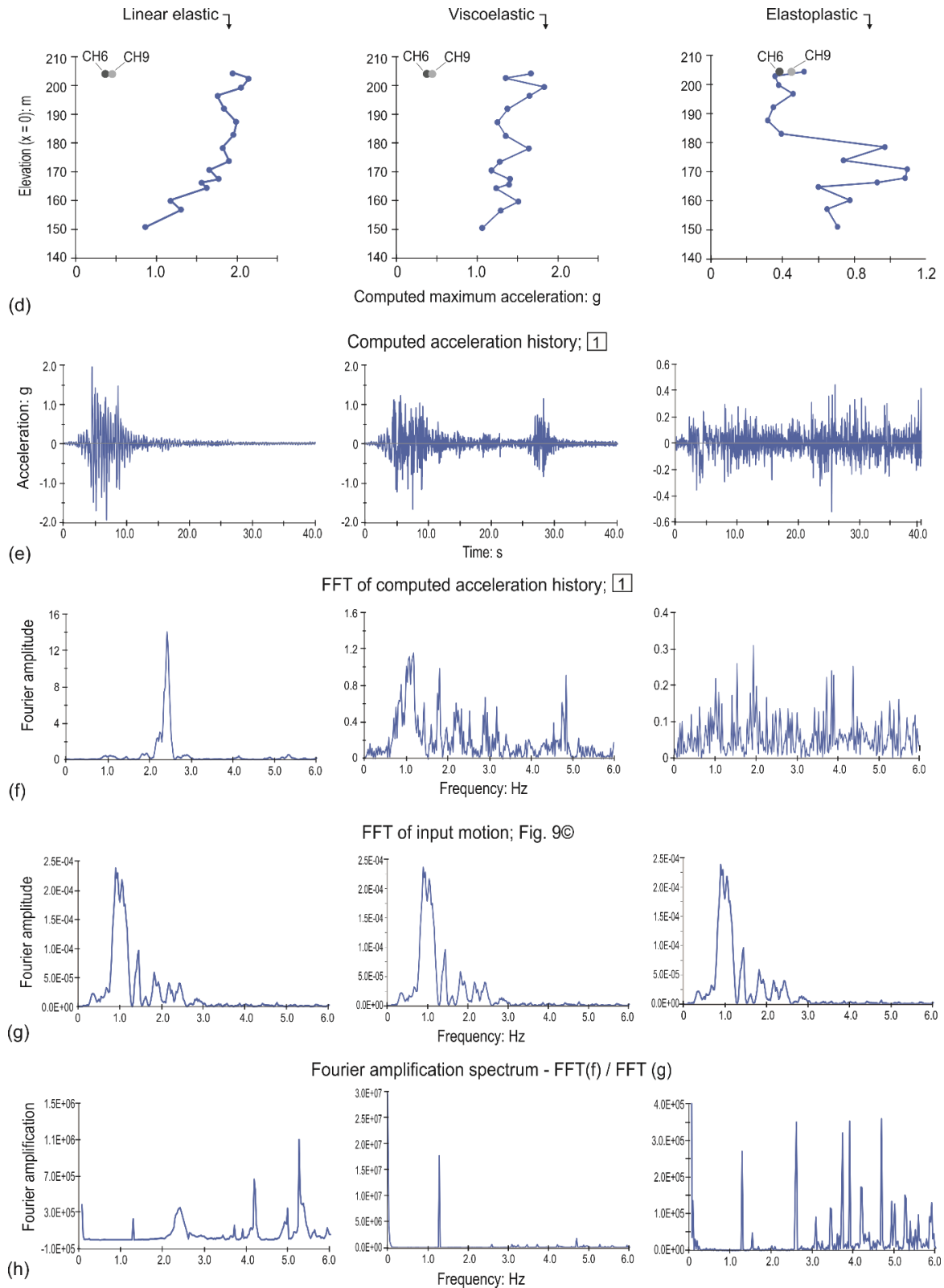
Figure 12.   (Continued)
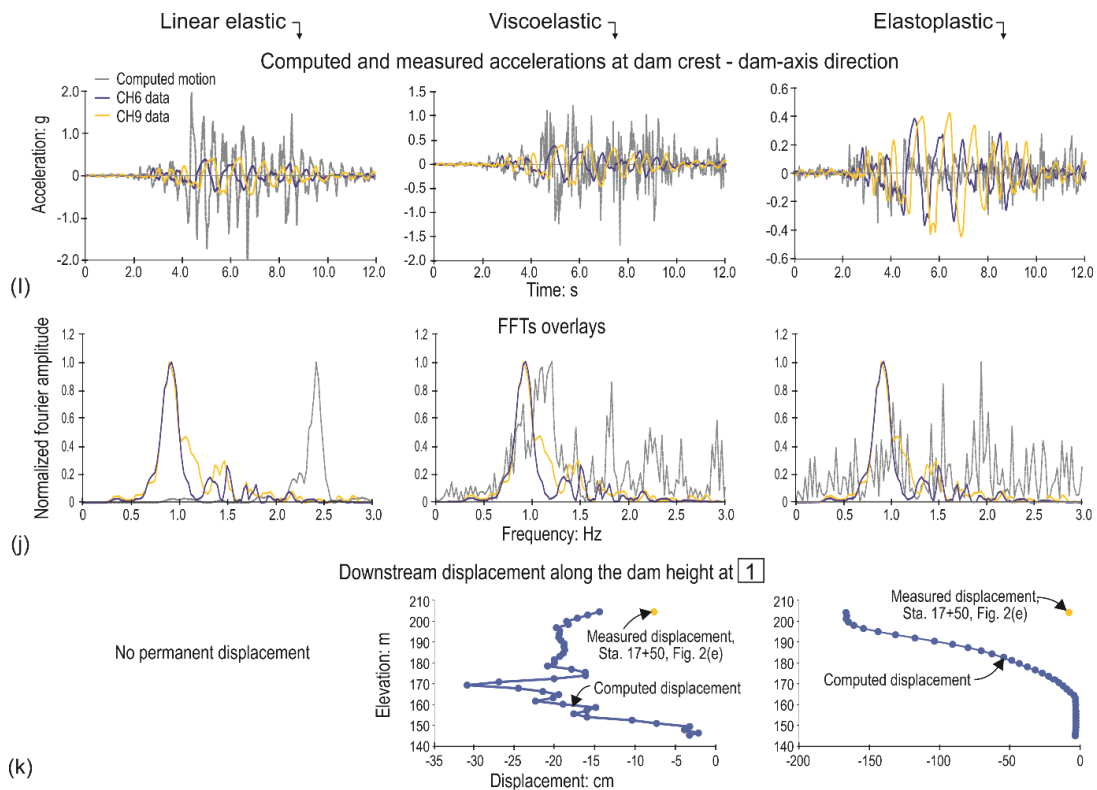
Figure 12.   (Continued)

Table 13   Frequencies corresponding to the spikes in the Fourier amplification spectrum plots, Fig. 12(h)

– Transverse section, continuum-based analyses

Material model	Frequency: Hz				
	f (p1)	f (p2)	f (p3)	f (p4)	f (p5)
Linear elastic	1.32	2.42	2.65	2.92	3.17
Equiv. linear	1.30	2.0	2.30	2.60	3.15
elastoplastic	1.30	1.55	1.80	1.87	2.02
1st Resonant frequency (Linear elastic)	2.40(dam-axis)	2.45(u/s-d/s)	3.2(vert)		

The overlays of computed motions and the recorded motions at the dam crest (CH6 and CH9) are shown in row (i) and the overlays of their FFTs (normalized to a Fourier amplitude of 1.0) are shown in row (j). The computed motions details compare poorly with those of the measured data.

There are no computed permanent displacements for elastic material model; the same for viscoelastic, and elastoplastic material models are shown in row (k) – these are permanent displacements of the dam crest near Stn. 17+50; the measured displacement in the transverse direction is included in (k). Obviously, the computed displacement is much larger than its measured counterpart.

Significant observations on deformation analyses results:

There are reasonable agreements and significant differences between the computed and observed performances of individual items as noted in the text of longitudinal and transverse sections. However, from a broad perspective, the computed results for all material models suggest that:

(1) The permanent deformations of the dam were affected by transitory matches between the frequencies of excitation waveforms and the prevailing natural frequencies of the dam at the time of the earthquake.

(2) The sustained durations of acceleration pulses in the seismic data (in the dam-axis and u/s-d/s directions) recorded at the two dam crest accelerometers and to some extent at the left abutment station location are taken to support this observation.

(3) In view of observation (2), it is fair to say that majority of the dam response occurred between about 5 to 10 seconds from the start of the seismic activity at the dam site.

6. Conclusions

(1) Linear elastic material models in two-dimensional plane strain analyses of longitudinal and transverse sections provide sharply demarcated tension zones in dams where potential cracks would be, if they were to occur, under static or seismic loading. For the Lexington Dam, the observed cracks, in terms of locations and depths, are well within the bounds of tension zones predicted by numerical means.

(2) Free and forced vibration analyses using linear elastic material in plane strain conditions provide useful information about the natural vibration characteristics of the dam-foundation-reservoir system which can be used in developing synthetic seismic motions or in prioritizing a few motions from the many developed (for different return periods) for detailed seismic analyses of the facility.

(3) Conclusions (1) and (2) can be used for existing and new dams to identify tension zones under prevailing or future load conditions, and remedial or preventive actions taken to minimize cracking before they cause significant or serious damages to the facility.

(4) For the Lexington Dam, computed permanent deformation in longitudinal and transverse directions did not compare well with the field data. It is most likely due to (i) the two-dimensional representations of the three-dimensional prototype with varying geometry of dam and foundation in a narrow 'V' shaped valley and (ii) the use of the empirical data for the cyclic stress-strain-damping characteristics as if they were representative of materials in the Lexington Dam.

(5) Selection of seismic instruments and their locations at a dam site requires expertise in seismology. It is ideal to have seismic instruments located near the base of the dam as well as at the dam crest and other convenient locations. At the Lexington Dam site, all three seismic stations were located near the dam crest elevation which proved to be a less-than-ideal combination of locations as it left the selection and use of recorded data for input motion up to the discretion of the analyst. For the analyses of Lexington Dam, the left abutment instrument data in the dam-axis and upstream-downstream directions were deconvolved to the base of the dam; the recorded data in the vertical direction were not used in the analyses. In general, seismic instrumentation program for a dam site should be a joint effort between an engineering geologist, a seismologist, and an engineer.

(6) The free and forced vibration procedure used for determination of frequencies and mode shapes provides an effective and efficient alternative to solving an eigenvalue problem. It is perhaps the only numerical means to calculate vibration characteristics when explicit solution schemes are adopted for solving structural mechanics problems. Such was the case with the computer program FLAC used for the analyses of Lexington Dam. Forced vibration tests on prototype structures for the same purpose are time consuming and expensive.

(7) In general, seismic data, whether developed or recorded, are in time-domain (e.g., time-acceleration). The time-domain data can be converted to frequency domain (frequency-amplitude) via Fourier transform. The frequencies in the seismic data and their comparisons with natural frequencies of the dam (whether calculated or measured via field tests) provide useful information about the possible outcome of a lengthy dynamic response analysis of a facility. Such was the case in the case study of Lexington Dam.

(8) Linear elastic material model can be used to advantage for studying potential zones where subsurface cracks may be present or develop due to presence of (a) rigid penetrations (cutoff walls, outlet works conduits); (b) valley geometry shape; (c) dam zoning; (d) compressibility of foundation; and possibly other contributing features in existing or new dams. Preventive measures against developments of cracks and their relative merits can be studied prior to their causing dam incidents or failures.

(9) Results from use of more advanced material models and analysis procedures can be compared with the ones from linear elastic material model to develop better understanding of computed results. Complete reliance on computed results from use of advanced material model must be avoided.

(10) Use of plasticity-based material models is appropriate for studying problems where the response of a structure is dominated by shear stresses; use of linear or nonlinear elasticity material model is more appropriate to study problems where response is dominated by normal stresses. Use of nonlinear elastic material model(s) will be investigated in future studies.

(11) Liquefaction, seepage and piping related issues were not a consideration in this case study. Therefore, the lessons learnt from this study should be considered applicable to other earth and rockfill dams with similar conditions.

Supplemental material

Relative displacements of three observers, one at each of the three accelerometer locations, are presented in real time using two animations in graphics interchange format. The horizontal plane animation shows relative displacements along the dam-axis and u/s–d/s directions; the vertical plane animation shows relative displacements in the dam-axis and up-down directions.

Acknowledgements

References

1. Swaisgood, J. R. (2003). Embankment dam deformations caused by earthquakes. In proceedings: 2003 Pacific Conference on Earthquake Engineering: Paper Number 014. University of Canterbury, Christchurch, NZ. https://www.nzsee.org.nz/db/2003/Contents.htm
2. Reitherman R. (2011). Earthquakes and Engineers: An international history. Reston, VA: ASE.
3. Yu, L., Kong, X., and XU, B. (2012). Seismic Response Characteristics of earth and rockfill dams. In proceedings: 15th World conference on Earthquake Engineering, Lisbon, Portugal: September 24 – 28, 2012.
4. Harder, L. F. (1991). Performance of earth dams during the Loma Prieta Earthquake. In Proceedings of the Second International Conference on Recent Advances in Earthquake Engineering and Soil Dynamics: March 11-15, 1991, St. Louis, MO; pp. 1613 - 1629.
5. Makdisi, F. I., Chang, C. Y., Wang, Z. I., and Mok, C. M. (1991). Analysis of the Recorded Response of Lexington Dam during various levels of ground shaking. In proceedings of the Seminar on Seismological and Engineering Implications of Recent Strong Motion Data, California Division of Mines and Geology, Sacramento, CA; pp. 10 – 1, 10 – 14.
6. Mejia, L. H., Sun, J. I., Salah-mars, S., Moriwaki, Y., and Beikae, M. (1992). Nonlinear dynamic response analysis of Lexington Dam. In proceedings of the Seminar on Seismological and Engineering Implications of Recent Strong Motion Data, California Division of Mines and Geology, Sacramento, CA; pp. 10–1, 10–14.
7. Hadidi, R., Moriwaki, Y., Barneich, J, Kirby, R., and Moores, M. (2014). Seismic deformation evaluations of Lenihan Dam under 1989 Loma Prieta Earthquake. In proceedings of the Tenth U.S. National Conference on Earthquake Engineering: July 21-25, 2014, Anchorage AK.
8. Dawson, E. and Mejia, L. (2021). Three-dimensional analysis of Lenihan Dam for the Loma Prieta Earthquake. In Proceedings of the United States Society on Dams 2021 Annual Meeting and Conference.
9. Aguilera, J. (2006). Documentation of visible damage to Lexington Dam following the Loma Prieta Earthquake of October 17, 1989. Santa Clara Valley Water District, San Jose, CA.
10. Jones, S. (2006). Review of performance during the Loma Prieta earthquake James J. Lenihan Dam, No. 72-8, Santa Clara County. Division of Safety of Dams, Department of Water Resources, Sacramento, CA.

11. Kirby, R. and Harlan, R. (2010). Seismic stability evaluations. Technical Memorandum Number SSE2–TM–1LN. Terra / GeoPentech, Irvine, CA.

12. Chugh, A. K. (1985). Dynamic response analysis of embankment dams. International Journal of Numerical and Analytical Methods in Geomechanics, 9 (2): 101-124.

13. Itasca Consulting Group (2011). FLAC – Fast Lagrangian Analysis of Continua.   Minneapolis, MN

14. Schnabel, P. B., J. Lysmer, and H. B. Seed. (1972). SHAKE: A computer program for earthquake response analysis of horizontally layered sites. Report No. UCB/EERC-72/12. Earthquake Engineering Research Center, University of California, Berkeley, CA.

15. USBR (1976). Dynamic analysis of embankment dams. U.S. Bureau of reclamation, Engineering and Research Center, Denver, CO.

16. Rea, D., Liaw, C.Y., and Chopra, A. (1972). Dynamic properties of Pine Flat Dam. National Technical Information Center, Springfield, VA.

17. Erdik, M. B., Atalay, Oner M., Ylizliglillli, O., and Yilmaz, C. (1980). Dynamic tests on Keban dam. Report No. DMAE 80-02. Directorate of State Hydraulic Works, Government of Turkey, Ankara, TR.

18. Chopra, A. K. (2008). Dynamics of structures. Prentice-Hall of India. New Delhi, IN.

19. Covarrubias. S. W. (1969). Cracking of earth and rockfill dams – a theoretical investigation by means of the finite element method. Ph.D. dissertation, Harvard University, Cambridge, MA. https://usace.contentdm.oclc.org/digital/collection/p266001coll1/id/3166/rec/22

20. Casagrande, A. and Covarrubias (1970). Cracking of earth and rockfill dams – tension zones in embankments caused by conduits and cutoff walls. Harvard University, Cambridge, MA. https://usace.contentdm.oclc.org/digital/collection/p266001coll1/id/7187/rec/23

21. He, K., Song, C., and Fell, R. (2021). Numerical modelling of transverse cracking in embankment dams. Computers and Geotechnics: 132 (4) – 104028.

22. CSMIP (2022). California strong motion instrument program, Available at the web address: www.strongmotioncenter.org/cgi-bin/CESMD/Multiplesearch1_DM2.pl?event_name=&magmin=&magmax=&byear=&eyear=&stn_ident=&type=D&Mat erial=Any&Height=&accmin=&accmax=&hdistmin=&hdistmax= Station no. 57180; Los Gatos – Lenihan Dam. [accessed 1 August, 2022].

23. COSMOS (2022). Strong-motion virtual data center – Global component of the center for engineering strong motion data. https://www.strongmotioncenter.org/vdc/scripts/plot.plx?stn=459&evt=24

24. Hudson, D. E. (1970). Grounf motion measurements. Earthquake Engineering, R. L. Wiegel (ed), Chapter 6. Prentice Hall, Englewood Cliffs, NJ.

25. USGS (2003). The Loma Prieta, California, earthquake of October 17, 1989 – geologic settings and crustal structure. Professional paper 1550-E, Denver, CO.

26. Seed, H. B., and Idriss, I. M. (1970). Soils modulii and damping factors for dynamic response analysis. Report No. UCB/EERC – 70/10. Earthquake Engineering Research Center, University of California, Berkeley, CA.

27. Chugh, A. K. (2007). Natural vibration characteristics of gravity structures. International Journal of Numerical and Analytical Methods in Geomechanics, 31 (4): 607-648.

28. Idriss, I. M. and Sun, J. I. (1992). User's manual for SHAKE91. Center for Geotechnical modelling, Department of Civil Engineering, University of California, Davis, CA.